DIAGNOSIS OF SEVERITY LEVEL OF DIABETES RETINOPATHY USING MULTISCALE FEATURE EXTRACTION

BY

MUHAMMAD, Yunusa Jimada Gana

MTech/SICT/2019/9856

A THESIS SUBMITTED TO THE POSTGRADUATE SCHOOL, FEDERAL UNIVERSITY OF TECHNOLOGY, MINNA, NIGERIA IN PARTIAL FULFILMENT OF THE REQUIREMENTS FOR THE AWARD OF THE DEGREE OF MASTERS OF TECHNOLOGY (M.TECH) IN COMPUTER SCIENCE

JULY, 2023

ABSTRACT

A common diabetes consequence called diabetic retinopathy (DR) affects the retina's blood vessels, a tissue that is sensitive to light. It is one of the most common causes of eyesight loss in older adults with diabetes. Since early medication can dramatically

reduce or even eliminate vision loss, DR severity level diagnosis is crucial. Unfortunately, most DR detection and classification algorithms ignore the multi-scale structure of images and instead concentrate on single fixed-scale picture attributes for prediction. Scale refers to the level of detail in an image. Although objects in medical images often come in various shapes and sizes, the constant input scale will restrict the effectiveness of spatial feature integration and prevent scale-dependent features from being gathered. These issues can be resolved by combining characteristics from several scales with scale-dependent data from the DR image. This study therefore proposes a multi-scale feature descriptor technique for DR classification, which solves the drawbacks of a single-scale approach while significantly enhancing classification performance. The proposed multi-scale features were developed by combining three different scales using a Gaussian pyramid. The three produced scales' features were extracted using the Local Binary Pattern (LBP) extractor. The obtained characteristics were fed into Decision Tree (DT) and Error-Correcting Output Codes (ECOC) classifiers for training and prediction. The proposed Multi-scale Feature Descriptor (MSFD) method was tested using the IDRiD dataset. The proposed MSFD technique provided an accuracy of 66.35%, which was better than the accuracy of 54.80% attained by the single-scale feature for DT prediction. Additionally, the novel method fared better than past research utilizing the IDRiD dataset. The obtained results for the accuracy, precision, recall and f-score indicate that the recommended approach can detect and evaluate different DR severity levels.

TABLE OF CONTENTS

LIST OF TABLES

LIST OF FIGURES

CHAPTER ONE

1.0 INTRODUCTION

1.1 Background to the Study

Diabetes is one of the most prevalent diseases in humans, leading to many complications across the world (Mangrulkar, 2018). Diabetes is a disorder of metabolism. The body uses glucose, which is created during food digestion, to produce the energy it needs. Digested food enters the blood stream with the aid of a hormone called insulin which is produced by the pancreas, an organ that lies near the stomach. During eating, the pancreas

automatically produces the correct amount of insulin needed for allowing glucose absorption from the blood into the cells (Amin et al, 2016). In individuals with diabetes, the pancreas either produces too little or no insulin or the cells do not react properly to the insulin that is produced (Selby & Taal, 2020). This leads to a build-up of glucose in the blood which overflows into the urine and then passes out of the body. Therefore, the body loses its main source of fuel though the blood contains large amounts of glucose (Ahmad et al, 2014).

Basically, there are three types of diabetes:

- Type 1 Diabetes, results from the auto immune problem. The body's immune system kills the pancreatic beta cells that produce insulin, which prevents the pancreas from making enough insulin (Bus et al, 2020).

- Type 2 Diabetes is a result of malfunctioning of the beta cell itself. This malfunction includes the non-production of insulin or a situation known as

insulin resistance. In insulin resistance persons, the muscles, fat and other cells do not respond to the insulin produced (Netten et al, 2020).

- Type 3 diabetes is known as gestational diabetes and only occurs during pregnancy. During this stage, the body resists the effect of the insulin produced (Amin et al, 2016).

Diabetes has a negative impact on the kidneys, eyes, nerves, and heart (Tarr etal., 2013). Diabetic Retinopathy (DR) is a diabetic complication that affects eyesight. It is a diabetes-related eye disorder in which the blood vessels in the retina enlarge and leak fluid, progressively impairing vision; its symptoms include blurred vision, eyespots, and night vision difficulties (Rajalakshmi et al 2018). It is one of the leading causes of blindness and vision loss in diabetics (Li et al, 2019). At early stage, DR may cause no symptoms or very moderate vision changes. Anyone with type 1 or type 2 diabetes can have this DR disease. Diabetes causes excessive blood sugar levels to collect in blood arteries, obstructing or inhibiting blood flow to the vital organs, including the eyes, and affects up to 80% of all people with diabetes for 10 years or longer (Tarr et al 2013). This assumption necessitates the application of automated diagnostic screening methods to larger populations for early detection of the disease. Research has shown that early detection of DR and regular eye examinations and therapies could prevent vision loss and blindness due to the disease (Ganesan et al 2014).

Experienced optometrists or highly skilled eye technicians conduct retinal screening for early detection of DR using retinal fundus photos acquired with mydriatic or nonmydriatic cameras (Rahimy, 2018; Sandhu et al 2018). However, this traditional

and manual DR screening is difficult to perform and is subject to significant inter- and intra-observer variation, even among experienced ophthalmologists: this can lead to erroneous interpretation, a delay in appropriate diagnosis, and a strain on healthcare services (Arcadu et al, 2019; Sandhu et al, 2018; Sarki et al, 2020). Automated detection of DR is required to address the issues of significant inter and intra-observer variation amongst ophthalmologists, which can lead to inconsistencies in interpretation, a delay in appropriate diagnosis, and a strain on health-care resources. The invention of intelligent systems to aid ophthalmologists in decision-making has drawn attention from the scientific community in a number of publications about inaccurate diagnosis (Islam et al, 2017; Pak et al, 2020). Lots of researches have been carried out on diagnosis of DR. However, most of the research focused on early-stage DR diagnosis rather than taking into account the stage of DR proliferation. In this research the stages of DR proliferation will be considered.

1.2 Problem Statement

It is becoming increasingly clear that the format used to represent image data can be as critical as the algorithms applied to the data in image processing. Most filters and feature descriptors used for diabetic retinopathy identification and classification are applied to the fundus image at a fixed scale, while image features occur at different scales. The fixed input scale limits the effectiveness of spatial feature integration and fails to capture scale-dependent information, although items in medical photographs commonly appear in various forms and sizes. Recent works on DR identification using deep neural networks and shallow learning

are still focused on extracting the DR features at a fixed scale while ignoring the multi-scale nature of images (Arcadu etal., 2019; Gulshan etal., 2016; Tymchenko etal., 2020). In order to solve these issues, a novel Multi-Scale Feature Descriptor (MSFD) is employed for DR identification at the various proliferation stages. The MSFD combines the features of DR on several scales into a single feature vector leveraging on the retained spatial-frequency domain obtained by the Gaussian pyramid, the proposed model automatically extracts discriminative features at different spatial scales and locations, leading to superior feature representation. The proposed model is also computationally efficient, as pyramid filtering is faster than equivalent filtering done with a Fast Fourier Transform.

1.3 Aim and Objectives

The aim of this study is to develop a technique that will perform diagnosis of the severity level of Diabetic Retinopathy using multi-scale feature extraction.

The objectives of this study are to:

i.   Identify the challenges of existing diabetic retinopathy identification techniques and collect a dataset of retinal images with annotations of the severity level of diabetic retinopathy.

ii.   Develop a multi-scale DR classification model based on multi-scale feature extraction.

iii. Evaluate the performance of the technique in (ii) using the standard metrics like accuracy, precision, recall and F1-score evaluation.

1.4 Scope of the Study

This research focuses on the automatic diagnosis of the severity level of diabetic retinopathy using the multi-scale feature extraction technique. The feature extraction and classification were performed using Local Binary Pattern (LBP) without consideration of feature extractors like Histogram of Oriented Gradient (HOG), Photo Response Non-Uniformity (PRNU), speeded up robust features (SURF) and Scale-Invariant Feature Transform a (SIFT). The image classification was also performed with Decision Tree (DT) and Error-Correcting Output Codes (ECOC) without exploring other classifiers such as Stack ensemble, Naïve Bayes (NB), Decision Tree (DT) and K-Nearest Neighbour (KNN), Discriminate analysis (DA), and logistic regression. This thesis is also limited to the IDRiD dataset without considering other DR Dataset sources like e-ophtha, HRIS, DIARETDB1, DIARETDB0 and DRIVE.

1.5 Significance of the Study

The diagnosis of diabetic retinopathy is crucial in preventing visual impairment and blindness among diabetic patients. Multi-scale feature extraction is a promising approach for the detection of diabetic retinopathy because it can capture important visual information at different scales. However, the existing systems for the diagnosis of diabetic retinopathy using single-scale feature extraction have some limitations, such as low accuracy. This study aims to address these limitations by developing an efficient system for the diagnosis of the severity level of diabetic retinopathy using multi-scale feature extraction. The proposed system is expected to provide a more accurate and efficient diagnosis of diabetic

retinopathy, which can lead to better treatment outcomes and improved quality of life for diabetic patients.

Moreover, the study will contribute to the knowledge of medical image processing and computer-aided diagnosis systems. The use of multi-scale feature extraction is an innovative approach that can improve the accuracy of diabetic retinopathy diagnosis. The proposed system will also involve the use of machine learning techniques, which are increasingly being used in medical image analysis. This study will provide insights into the application of machine learning techniques for the diagnosis of diabetic retinopathy and can serve as a foundation for future research in this area.

Finally, the proposed system has the potential to make a significant impact on the healthcare system, particularly in developing countries where access to eye care services is limited. The use of an automated system for the diagnosis of diabetic retinopathy can improve the efficiency of eye care services and reduce the burden on healthcare providers. This can also result in cost savings for patients who would otherwise need to travel to a specialist for diagnosis. Overall, this study has the potential to contribute to improved healthcare outcomes for diabetic patients, particularly in resource-limited settings.

1.6 Organization of the Thesis

This thesis is divided into five chapters, beginning with Chapter one, and ending with Chapter five. The first chapter provides an overview of the research project. It also includes problem statements, goals and objectives, the scope of the research,

and the significance of the research. Chapter 2 describes diabetic retinopathy in depth and analyses past studies on the subject undertaken by various researchers. The methods utilized to analyze the topic are discussed in Chapter 3. It supports the method for obtaining a solution to the problem. It goes over data collecting methods, feature extraction, and classifier ensemble. The details of the actual experimentation and the outcomes are presented in Chapter 4. Finally, Chapter 5 presents the summary of the work, the conclusions reached and the recommendations for future work.

CHAPTER TWO

2.0 LITERATURE REVIEW

2.1 Diabetic Retinopathy Disease

Diabetes mellitus is a sugar metabolic disease characterised by high blood glucose levels and caused by inadequate insulin secretion (Ahmad et al 2014). Hyperglycaemia can harm the arteries that provide blood to vital organs (high blood glucose levels). DR is a diabetic complication that affects the vascular system of the retina, resulting in slow retinal degeneration and vision loss. DR is the leading cause of blindness among the working-age population (Al Hazaimeh et al 2018). Diabetes has been identified as a significant developing global public health threat (Banu et al 2016); In the United Kingdom, 3 million people are estimated to have diabetes, with the number anticipated to double in the next 15- 30 years (Public Health England, 2016). In the year 2000, 171 million individuals

were predicted to have diabetes worldwide, with that number expected to climb to 366 million by 2030 (Dutta etal., 2018). Laser therapy can help prevent visual loss if DR is detected early enough (Sopharak et al, 2010). When the DR is still in its early stages, interventions like improved blood glucose control may be able to assist slow its progression (Romero-Aroca, 2015). Because DR often has no signs or symptoms, screening is essential for diagnosis. Once DR has been identified, patients can be treated correctly with the goal of preventing vision loss (Priyanka & Virani, 2017).

The retina is a light-sensitive tissue that runs along the eye's interior surface. Thousands of photoreceptors in the retina react to focused light and convert it to electrical messages. These signals travel through the optic nerve to the brain, where they are translated into images. The retina includes the retinal blood vessels, macula, optic disc, and fovea (Priyanka & Virani, 2017). Because of its huge number of cone cells, which are responsible for fine visual acuity, colours, and centre vision, the macula consumes a major percentage of the brain's visual capability. The fovea, which is positioned in the macula's centre, has the highest number of cone cells (W. Wang & Lo, 2018).
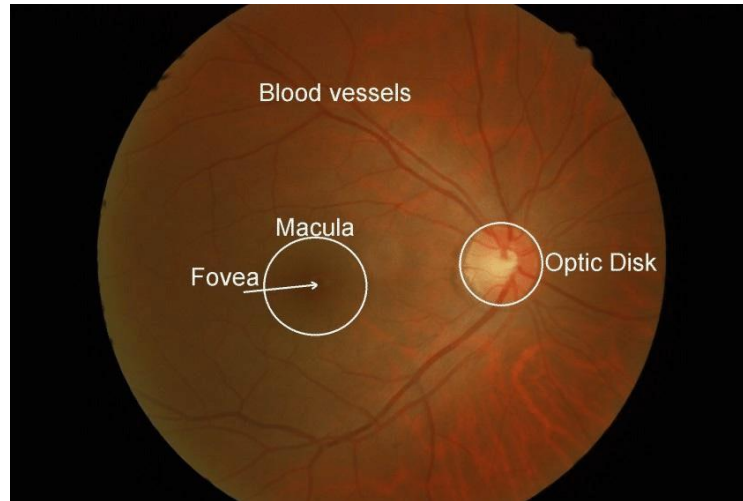
Figure 2. 1 Retinal structure: Blood vessels, Optic Disk, and Fovea/Macula (Basit & Egerton, 2013)

DR is a microangiopathy that affects the retinal vasculature caused by hyperglycaemia. Microaneurysms, exudates, haemorrhages, cotton wool patches, and venous loops occur when blood and fluid escape from injured retinal blood vessels (Tarr etal., 2013). Because DR is a degenerative disease, regions of retinal ischemia develop when blood vessel obstructions and damage worsen. In an attempt to re-vascularise the area, the development of new blood vessels is triggered. New vessels indicate the final stages of DR, providing a high risk of long-term vision loss because to their sensitive nature and the chance of significant bleeding. The key components of DR are discussed in further depth in the subsections below, along with images.

2.1.1 Microaneurysms

Microaneurysms are balloon-like structures that grow on the margins of capillaries as the walls weaken. Because capillaries are not visible on standard fundus imaging, microaneurysms show as single red dots unconnected to any blood artery.

9

They're often the first signs of DR that people notice (Somasundaram & Alli, 2017). Figure 2.2 depicts microaneurysms in the retina.
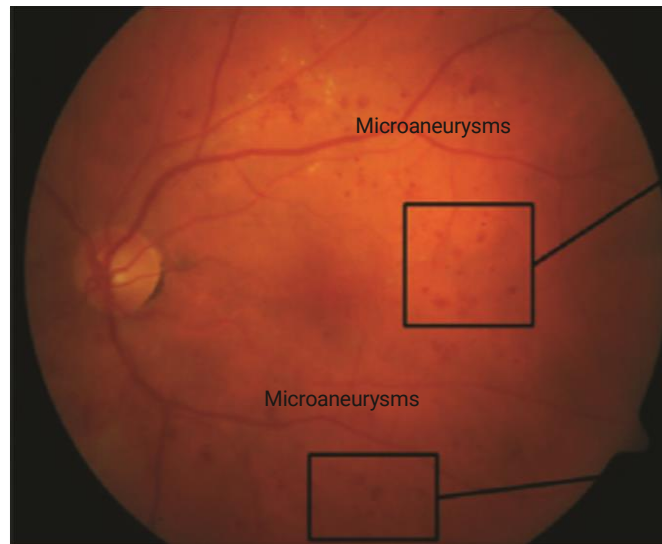
Figure 2. 2 Microaneurysms in retina image (Amin et al 2016)

2.1.2 Haemorrhages

The breaking of capillary walls, which can vary in size and shape depending on the retinal layer in which the capillaries are located, causes blood to spill (Li et al 2020). Haemorrhages, also known as retinal haemorrhages, are small or large areas of bleeding in the retina. They are caused by the leakage of blood from damaged blood vessels in the retina, and are a common feature of diabetic retinopathy (Benger et al 2020). The appearance of haemorrhages can range from small dots to large blotches, and their location and extent can provide important information about the severity of diabetic retinopathy (Amin et al 2016). The presence of multiple haemorrhages can indicate more advanced disease and a higher risk of vision loss. In some cases, haemorrhages can resolve on their own,

while in other cases they can cause permanent damage to the retina and lead to vision loss (Park et al 2021). A retinal image with haemorrhages is shown in Figure 2.3.

Figure 2.3 Haemorrhages in Retina Image (Amin et al 2016)

2.1.3 Exudates

Capillary collapse is a common cause of oedema leakage. Oedema builds up in the retina, causing it to thicken. In diabetics, macular oedema is the most prevalent cause of vision loss, and if it is medically severe, laser therapy will be required to

prevent visual loss (Dutta etal., 2018). Oedema is a clear fluid that is invisible on traditional 2D retinal imaging. The lipid leftovers of the oedema are known as exudates (Guo etal., 2020; Theera-Umponetal., 2020). As waxy yellow lesions with a variety of designs, isolated patches, track lines, macular stars, and circinates emerge. There are two types of exudates: hard and soft exudates (Auccahuasi et al 2020).
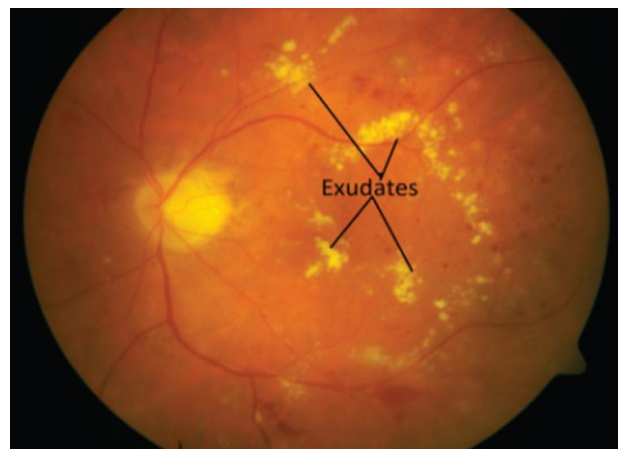
Figure 2.4 Exudates in Retina Image (Sariera et al 2019)

1. *Hard Exudates:* Hard exudates are yellowish-white lipid deposits that can accumulate in the retina, particularly in the macular region (Liu etal., 2022). These are a common symptom of DR and can range in dimension from

microscopic dots to big spots with defined boundaries. In addition to blood, the eye contains liquid that is high in protein and fat, which leaks out to produce exudates. These can make it difficult to see because they block light from getting to the retina (Kurilová et al, 2021) .Hard exudates can cause damage to the macula, the central part of the retina responsible for clear, sharp vision, and can lead to vision loss. Their presence is often used as a criterion for the severity of diabetic retinopathy, with a higher number of hard exudates indicating more advanced disease (C. Huang et al, 2021).

2. *Soft exudates:* Soft exudates, also known as cotton wool spots, are fluffy white or greyish lesions that can occur in the retina (Mateen et al, 2020). They are caused by the accumulation of axoplasmic material in the nerve fibre layer of the retina, which is often associated with damage to the blood vessels. Soft exudates are a common feature of diabetic retinopathy and are considered an early sign of the disease. They can be used to assess the severity of diabetic retinopathy, with a higher number of soft exudates indicating more advanced disease (Lin et al, 2020).
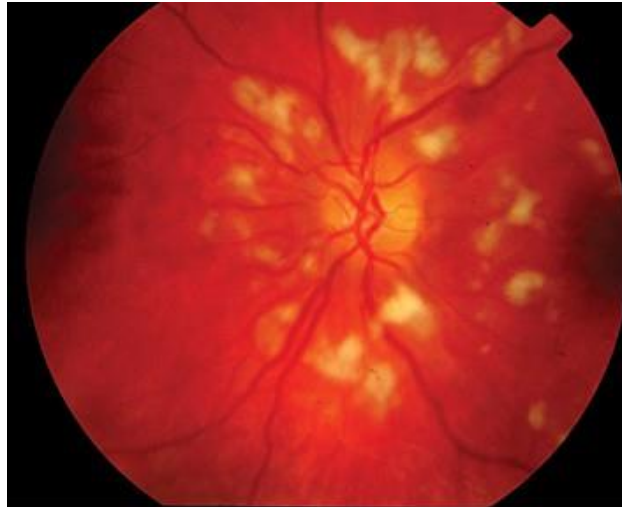
Figure 2. 5 Soft Exudates in Retina Image (Sopharak et al, 2010)

2.1.4 Neovascularisation

Neovascularisation refers to the formation of new blood vessels. In the context of diabetic retinopathy, neovascularisation refers to the abnormal growth of new blood vessels in the retina or optic disc. These new vessels are fragile and can leak blood and fluid into the retina, causing vision loss and damage to the retina (Rahman et al, 2021; Tang et al, 2021).

This condition is marked by abnormal blood vessel proliferation in many areas of the eye, particularly the retina, and is associated with blindness (Kesidou et al,

14

2020; Nicholas & Mysore, 2021). Ischemia, or a loss of blood supply to the ocular tissues, causes this to develop. If these abnormal blood vessels form around the pupil, increasing the stress within the eye, glaucoma can develop (L. Chen et al, 2020). These new blood vessels have thinner walls, making them more prone to rupture and cause haemorrhage, or to cause scar tissue to grow, dragging the retina away from the back of the eye. A retinal detachment occurs when the retina tears away from the back of the eye, and if left untreated, it can result in significant blindness (Tian etal., 2021). Blood leaks can obstruct the vitreous and hinder light from reaching the retina through the pupil, resulting in distorted and hazy visions. Diabetic fibrous may grow on the retina in more advanced proliferate retinopathy (Tarr et al, 2013).

2.2 Stages of Diabetic Retinopathy

The stages of DR are summarised in Table 2.1. The four basic kinds of DR are Background DR, Proliferative DR, Pre-proliferative DR, and Maculopathy. Background DR is the mildest type of DR and has no effect on vision. Pre-proliferative DR is a form of progressive retinal ischemia that has a high risk of neovascularisation. Neovascularisation is a hallmark of proliferative DR, and it is the most dangerous stage of the disease, with a high risk of vision loss. Table 2.1 shows that proliferative DR includes properties other than new vasculature, nevertheless, keep in mind that these additional features are due to the presence of new vessels. Maculopathy can occur at any stage of the disease, although it is more common as the disease progresses. The official definition of maculopathy is the presence of any DR features at the macula, but this is usually reserved for

vision-threatening macular oedema (Oloumi et al, 2014).

Table 2.1 Classification of DR

Stages of DR	Features
Background	Microaneurysms
	Dot and blot haemorrhages
	Exudates
Pre-proliferative	Multiple dot and blot haemorrhages.
	Cotton wool spots (CWS).
	Venous beading and loops.
	Intra-retinal microvascular abnormalities (IRMA).
Proliferative	New vessels elsewhere (NVE).
	New vessels at the disc (NVD).
	Pre-retinal/vitreous haemorrhage.
	Retinal detachment.
Maculopathy	Microaneurysms, haemorrhages, exudates at the macula.
	Macular oedema.

2.3 Diabetic Retinopathy Detection Methods

In recent decades the topic of retinal photo analysis has drawn a lot of attention, with the automated detection of diabetic retinopathy receiving a lot of it. Another topic that has drawn a lot of attention is landmark identification (Çeliktutan et al., 2013; Scherhag et al, 2018). The fovea, the optic disc, and blood vessels are all landmarks. The first part of this section will provide a brief review of computerized

blood vessel segmentation. Before detecting sick entities, most DR detection procedures, notably new vessel detection methods, require it as a precondition (Spencer et al, 1996). A brief review of the various methodologies for detecting the important DR traits (microaneurysms, haemorrhages, and exudates) will be presented. After that, there will be a section that contains a full report on the discovery of additional vessels (proliferative DR). The final section of this chapter provides a concise overview of the Machine Learning algorithms discussed throughout this literature review. Pre-processing the photographs is the first step in most processes. To adjust for low illumination and contrast, the basic pre-processing methods are applied. When coping with low lighting, shade adjustment is a typical solution (Niemeijer et al, 2005), whereby an image resembling the background is deducted from the initial image. The background image is created by using a median filter with a size that is much larger than the largest retinal feature. Contrast limited adaptive histogram equalization (CLAHE) is a common solution for poor contrast (Ramlugun et al, 2012). This is a way for improving local contrast that is preferable to increasing global contrast. Pre-processing on the other hand, can only help to a certain level; as a result, it is the photographer's responsibility to capture photographs of an acceptable standard. The pre-treatment procedures for retinal analysis are described in depth by (Youssif etal., 2007).

2.3.1 Vessel Segmentation

Vessel segmentation is a technique used in medical image analysis to separate blood vessels from the background and other structures in an image, such as

retinal images, angiograms, and magnetic resonance imaging (MRI) scans (D. Wang et al 2020). The segmentation process is an important step in vessel tracking, quantification, and diagnosis of vascular diseases (Ma et al., 2021; Park et al 2020).

The segmentation process can be done using different techniques, such as thresholding, edge detection, region growing, and machine learning-based methods. Thresholding is a simple method that involves selecting a threshold value to separate the vessel from the background based on the pixel intensity (Khan et al., 2022). Edge detection methods use mathematical algorithms to detect the edges of the vessels and separate them from the background (Haoran et al 2019). Region growing methods start from a seed point and grow a region that belongs to the vessel based on some similarity criteria, such as intensity or texture (Wisaeng & Sa-Ngiamvibool, 2018).

The rich red hue of vessels, their contrast with the background, and their gradient at vessel borders are all important characteristics that are used in segmentation algorithms (Cree et al 2005). Their cross-section intensity profile resembles a Gaussian function and can be approximated as piecewise linear. Different methods have been published in the literature, and they can be divided into four categories based on mathematical morphology, matched filtering, vessel tracking, and machine learning. Fine, weak, and highly convoluted vessels might be difficult to find using vascular segmentation algorithms. The profile model can be complicated by vessel crossing and branching. Vessels can have high reflections along their midline, complicating the profile model even more. Pathologies can

potentially reduce precision, resulting in false positives. On a pixel-by-pixel basis, vessel segmentation approaches are evaluated (Yin et al 2012).

2.3.2 Vessel tracking

Vessel tracking is a technique used in medical image analysis to detect and track blood vessels in various imaging modalities, such as fundus photography, retinal angiography, and optical coherence tomography (OCT). The tracking process involves identifying the position, orientation, and curvature of vessels over time or across different images (Ganesan et al 2020; Jia & Zhuang, 2021).

The vessel tracking process typically involves several steps, including pre-processing, vessel segmentation, vessel centreline extraction, and vessel tracking. Noise reduction, picture normalisation, and contrast enhancement are procedures taken during pre-processing to increase the precision of vessel segmentation (Zhou et al 2020). The process of segmenting an image's vessels using techniques like thresholding, edge detection, and region growth allows us to distinguish them from the image's backdrop and other features. The centrelines of the vessels can be extracted after they have been segmented using methods like skeletonisation, medial axis modification, or geometric deformable models. The vessel's position and orientation throughout its length are represented by the centrelines, which can also be used to calculate the diameter, tortuosity, and bifurcation angle of the vessel (Widyatmoko etal., 2021).The tracking results can be used to analyze vessel dynamics and pathology, such as changes in vessel diameter, blood flow, and vessel density.

Cree etal.(2005) used a two-dimensional Gaussian framework to track vessels. A starting vessel point, as well as estimates of its breadth and direction, had to be manually picked. A tiny local area was removed around this point, and a Gaussian model with the same breadth and alignment was fitted by the non-linear least square's optimisation approach. The fitted model was used to take precise measurements of vessel width and alignment. A tiny step was taken toward the vessel, and earlier dimensions were used as approximations to create a new fitting. Additional methods include a vessel tracking technique founded on utilizing a probabilistic design (Yin et al, 2012) and a method based on multi-scale line tracking (Vlachos &Dermatas, 2010).

2.3.3 Matched filtering

Matched filtering is a signal processing technique that is used to detect a known signal, or a pattern, in noisy data. The basic idea behind matched filtering is to convolve the input signal with a filter, known as the matched filter that is designed to maximise the signal-to-noise ratio of the output (Ahmadi et al,2021).

The matching filter is applied to the input image to emphasise the regions that contain the desired pattern and is made to match the properties of the object or feature of interest (Kato & Nakagawa, 2020; Southwell et al, 2020).Matching filtering can be used in the context of medical imaging to identify specific structures or abnormalities, such as tumours, lesions, or microaneurysms in retinal images for the diagnosis of diabetic retinopathy (Saroj etal., 2020). The filter can be created based on the properties of the desired structure, then used to enhance or detect the structure in the input image. After the regions of interest have been

located via matched filtering, they can be further examined using machine learning algorithms and other image processing methods to categorise the severity of a condition or arrive at a diagnosis (McGuire et al 2021).

Chaudhuri et al.(1989) proposed the matched filter for vessel segmentation, and it has since become one of the most widely used methods. It made use of the knowledge that a Gaussian function may be used to estimate the cross section of vessels, as well as the idea that vessels can be conceived of as piecewise linear segments. As a result, a two-dimensional Gaussian filter was used, which differed from a traditional isotropic Gaussian filter in that a single Gaussian function transverse profile was replicated and packed several times to make up the filter's length. The length of the filter was selected to be close to the distance at which vessel segments were considered linear. This filter, which matched the geometry of vessel segments, was coupled with the retinal picture to "match" the blood vessel segments. The filter was also adjusted to recognise vessels of varied orientations. As a result, the matching filter response (MFR) was developed, resulting in a vastly better image. The binary vessel map was then created using a global threshold.

Al-Rawi et al. (2007) improved the effectiveness of the matched filter by using an optimisation technique to automatically determine the best filter parameters. Unfortunately, the matched filtering method reacts to non-vessel edges as well as vessel edges. A single global MFR threshold is insufficient, and multiple false positives can result. As a result, a variety of modified matched filtering methods have been proposed.

Hoover (2000) suggested a piecewise threshold probing strategy based on vessel structural information. The program looked at the MFR and used a set of criteria to determine the threshold for each place so that vessels could be segmented during each probe. Zhang et al (2009) used the point that the MFR highest point for a vessel is significantly superior to its surrounding points on either side; however the MFR peak point for non-vessel edges is not significantly superior to its neighbours on either side. A two-sided thresholding method was presented as a result.

2.3.4 Machine Learning Methods

Machine learning is a branch of study that focuses on the creation of models and algorithms that allow computers to learn from data and make decisions without being explicitly programmed. Machine learning aims to create systems that can automatically learn from experience and get better without having to be explicitly coded for each task (Theeng et al 2020).

The three broad categories of machine learning algorithms are reinforcement learning, unsupervised learning, and supervised learning. In supervised learning, each data point has a label or target value, and the system is trained on this labelled data. Based on the patterns and relationships found in the training data, the algorithm learns to predict outcomes for new data (Cholaquidis & Fraiman, 2018; Ward, 2019).

Unsupervised learning involves training the algorithm on unlabelled data with the aim of revealing hidden patterns or structure in the data (Basar etal., 2020; Sathya & Abraham, 2013). Common applications of unsupervised learning include

clustering and dimensionality reduction. In reinforcement learning, the algorithm learns to make choices based on a signal of rewards, with the aim of maximising the cumulative reward over time (Hammoudeh, 2018). Robotics and control systems frequently employ this kind of learning (R. Sharma, 2013).

Image pixels are classified as vessel or non-vessel in the machine learning method. This categorisation employs both supervised and unsupervised learning techniques.

1. **Supervised Learning:** Sinthanayothin etal.(1999) used principal component analysis (PCA) to limit the photo to simply structural detail. To quantify edge strength, the canny edge detector was applied to the first principal component. The first principal component values and edge strong point were used as input data for a neural network classifier. The method utilised by Staal etal (2004) was to extract ridges, which were then used to create photo primitives in the shape of line components. The image was then divided into patches using these line elements. A vector of 27 characteristics obtained from qualities of the spots and line components were used to categorise pixels using a KNN algorithm. (Soares etal. 2006) produced a feature vector for each pixel based on the intensity of the pixel and the response of a two-dimensional Gabor wavelet applied at various measures and alignments. A Bayesian classifier was used to classify pixels, with class likelihoods given as a linear combination of Gaussian functions.

2. **Unsupervised:** Tolias and Panas (1998) proposed an unsupervised fuzzy technique for vessel tracking. The membership functions of the two

linguistic values were discovered using a fuzzy C-means clustering approach (vessel and non-vessel). No hypotheses regarding the shape of the vessels were established, and no edge information was necessary, because the suggested solution relied entirely on intensity data (usually corrupted by noise). Kande et al (2010) used matched filtering to boost the contrast of blood vessels against the background. The improved image was labelled using a spatially weighted fuzzy C-means clustering algorithm to segment the vessels. The spatial weighting component considered the fact that photo intensity and grey level spatial distributions are not independent of one another.

2.3.5 Mathematical Morphology

Mathematical Morphology is a field of image processing that deals with the analysis and manipulation of geometric structures in images. It uses mathematical operators, such as dilation, erosion, opening, closing, and others, to extract and analyze image features related to the shape and structure of objects in the image (T. Chen et al, 2017).

The fundamental principle of mathematical morphology is to treat an image as a set of points and to change the size and shape of the sets of points that represent objects or features in the image using mathematical operations. For instance, dilation can be used to make objects in the image's boundaries larger, erosion can be used to get rid of small things, and opening and closure can be used to fill in any gaps and smooth up boundaries (Rodrigues &Marengoni, 2017).

Numerous image processing tasks, including edge detection, feature extraction,

object recognition, noise removal, and segmentation, can be accomplished using mathematical morphology. It is especially helpful in situations where the shape and organisation of visual objects are crucial, such as in computer vision, remote sensing, and medical imaging (Bauget al., 2017; Li et al 2017).

Mendonça and Campilho (2006) employed variance of offset Gaussian filtering to retrieve the vessel midline. Using a customized top hat operator with an expanding disc structural component, vessels of varying widths were boosted separately at various levels, returning to the previous pre-processed photo. At each scale, the double threshold operator was employed to perform morphological reconstruction, yielding a binary vessel map. Using the vessel mid-lines and multiple binary vessel maps, the final vessel segmentation was constructed through iterative region-growing. Fraz et al (2012) proposed an improvement on the work of Mendonça and Campilho (2006). The vessel mid-lines were found using the Gaussian kernel's first order derivative. Bit plane slicing was utilised to construct a binary vessel map once the top hat vessel enhanced image was acquired; the sum of the higher order bit planes was used to generate a binary vessel map.

2.4 The Retinal Image

Retinal image refers to an image captured of the inner surface of the eye, specifically the retina. It is often used for diagnostic purposes, such as for detecting and monitoring eye diseases like diabetic retinopathy, macular degeneration, and glaucoma (Valverde et al 2016; Verma et al 2011). Retinal imaging techniques include fundus photography, optical coherence tomography (OCT), fluorescein angiography, and scanning laser ophthalmoscopy (SLO)

(Manojkumaretal., 2019; Mohamed et al, 2017).

The amount of reflected light is represented by the image's intensity. A microscope with a camera connected to it makes up the eye fund camera. The optic system is comparable to that of an indirect ophthalmoscope, which allows for vertical and enhanced views of the inner surface of the eye. The camera records observations of the retina from a 30 to 50-degree angle, with a 2.5-fold amplification (Abramoff et al, 2010).

The test involves the use of colour filters, fluorescein, and other dyes. The retinal examination for DR detection is carried out using the methods listed below (Welikala, 2014).

1. **Fundus photography (red-free)**: The amount of light reflected by a given wavelength band is used to capture the image.

2. **Colour Fundus Photography**: Reflected light in the RGB (Red, Green, and Blue) spectrum is used to capture the image.

3. **Indocyanine and fluorescein angiography**: The number of photons emitted by the fluorescein or indocyanine dyes injected into the bloodstream is used to create the image (Patel et al, 2015).

Colour Fundus Photography was utilized in this project since it has a few advantages over the other approaches mentioned above. Only the green channel of the RGC fundus image is used in red-free fundus photography, which may result in the loss of valuable information. Fluorescein angiography, on the other hand, necessitates contrast injection, which increases the cost and invasiveness of the

procedure (Zago, 2019).

2.5 Related Works

In the world of computer vision, recognizing Diabetic Retinopathy (DR) early is a difficult problem. The goal of diagnosis is to detect clinical features of diabetes retinopathy using diagnostic clarity criteria. Haemorrhages, microaneurysms, soft exudates, and hard exudates are all clinical features of diabetes retinopathy in retinal fundus pictures. Extracting these symptoms is a critical difficulty for accurate diagnosis because they aid in determining the current stage of diabetic retinopathy.

Bilal et al (2021) proposed a novel hybrid approach for prior DR detection and classification. Distinctive models were combined to make DR detection robust based on majority voting method. The proposed work follows pre-processing feature extraction and classification steps. The pre-processing step enhances abnormality presence as well as segmentation; the extraction step acquires merely relevant features; and the classification step uses classifiers such as Support Vector Machine (SVM), K-nearest neighbour (KNN), and Binary Trees (BT). To accomplish this work, multiple severities of disease grading databases were used to achieve an accuracy of 98.06%, sensitivity of 83.67%, and 100% specificity. A drawback of the proposed technique is complexity. The model has high complexity as it costs more to create, train and deploy.

In the work by Kalyani etal.(2021), a reformed capsule network was developed for the detection and classification of diabetic retinopathy. Using the

convolution and primary capsule layer, the features are extracted from the fundus images and then using the class capsule layer and softmax layer, the probability that the image belongs to a specific class is estimated. The efficiency of the proposed reformed network is validated against four performance measures by considering the Messidor dataset. The constructed capsule network attained an accuracy of 97.98%, 97.65%, 97.65%, and 98.64% on the healthy retina, stage 1, stage 2, and stage 3 fundus images respectively. The limitation of the proposed capsule network is that the networks have higher complexity in implementation compared to Convolutional Neural Networks (CNNs). The proposed model is slow, mainly due to the inner loop of the dynamic routing algorithm.

Tymchenko et al (2020) proposed DR diagnosis on fundus images using multi-stage transfer learning. Three CNN architectures were combined. The CNN was employed as a feature extractor and a classifier. Imagenet-pretrained CNNs were employed as the encoder's seed. The proposed approach was employed as a screening means of early identification of DR, with a sensitivity and specificity of 0.99 percent. The Shapley Addictive exPlanations (SHAP) were used to characterise aspects that helped with disease stage assessment. Using SHAP ensures that the model learns helpful features during training and uses the proper features at inferential time. The main advantage of this strategy is that it enhances generalisation and reduces uncertainty by employing a network ensemble that has been trained on a large data set and fine-tuned on the target data set. This approach can be further enhanced by calculating SHAP for the full ensemble rather

than just a single network, resulting in a more precise hyper - parameter optimisation.

Li etal. (2019) presented a unique CNN technique. A fractional max-pooling layer was used in place of the conventional CNN max-pooling layers in this paper. To achieve additional discriminatory characteristics, two CNNs with different numbers of layers were created for categorisation. The Support Vector Machine (SVM) classifier was trained to discover the inherent limitations of distributions of each category after incorporating characteristics from image metadata and CNNs. The proposed DR technique divides diabetes retinopathy phases into five categories, each of which is labelled with a number ranging from 0 to 4. According to the test findings, the suggested technique can achieve an identification rate of up to 86.17%. The proposed technique was limited by the lack of images of lesions 3 and 4 in the training data set used in this investigation.

Zeng et al (2019) suggested a binocular Siamese-like CNN for automatic DR detection. The suggested method takes as inputs binocular fundus images and discovers their correlation to aid in forecasting. The model basically takes two fundus photos belonging to the left and right eyes as inputs and sends them to the Siamese-like modules. In the fully connected layer, the data from two eyes are integrated, and the model then produces the diagnosis result for each eye independently. In this study, the Kaggle DR Image dataset was employed. A total of 35126 high-resolution fundus pictures were obtained under a variety of imaging circumstances for the data set. The proposed binocular model performed well, with an area under the curve of 0.951, a recall of 82.2% and a specificity of 70.7%. The

suggested method has the disadvantage that binocular models will have difficulty training or validating with datasets that do not have feature paired fundus images.

Kirange etal.(2019) suggested a new method for detecting DR at an early stage by recognising all microaneurysms, the initial signs of the disease, and correctly labelling retinal fundus images, which are divided into five categories based on the severity of the lesions. This proposed system uses five standard classifiers to fulfil the classification task. SVM, KNN, Neural Networks (NN), Naïve Bayes (NB), and Decision Tree (DT) are the classifiers used. With an accuracy of 77.86%, the NB classifier was said to have outperformed the other four classifiers. The Gabor and LBP descriptors were both utilised to extract features. The Gabor descriptor features, fared substantially better than the LBP features, with an accuracy of 77.86% compared to 41.84% for the LBP features. One limitation of this study is that it concentrated only on early-stage DR detection rather than taking into accounts the stage of DR proliferation.

Costa et al (2018) established a novel Multiple-Instance Learning-based weakly-supervised DR diagnosis system. The method used inherent local information to generate predictions on new photos based on weak information about the absence or presence of the disease. The adoption of a joint-learning approach in which the encoding and classification phases are linked is the study's main contribution. SURF (Sped-Up Robust Features) were used to locate and define occurrences within retinal pictures in this study. The DR detection model was evaluated using the publicly available Messidor dataset. The proposed technique achieved an area under the curve of 90% on the Messidor dataset and 93% on the DR1 dataset. This

study was limited to just the SURF feature; however, exploring more features such as texture, deep learning and image degrading features could help describe the DR disease more effectively which would in turn improve the proposed systems' performance.

Al-Hazaimeh et al (2018) suggested an effective image processing method for detecting DR illnesses from retinal fundus pictures. Pre-processing, blood vessel segmentation and removal, optic disc detection and removal, fovea elimination, feature selection, feature extraction, and classification were all part of the proposed automatic screening method for DR. The proposed method was benchmarked using the DIARETDB1 publicly available dataset. The Grey-level co-occurrence matrices (GLCM) were used to extract the microaneurysm, retinal haemorrhage and exudates feature from the retina fundus images. Deep belief network was used to carry out feature selection. SVM model was adopted for data classification. The proposed technique was validated using sensitivity, specificity and accuracy performance metric. In this study an accuracy of 98.4%, sensitivity of 99% and specificity of 96% was achieved. The DIARETDB1 consist of 89 colour fundus images was used for training and testing the proposed method which makes the method limited to a small dataset size. Increasing the dataset size would produce a more robust model.

Sudha and Karthikeyan (2018) presented an analysis of DR using the Naïve Bayes classifier technique. There are 385 instances and 9 features in the collection. This data was obtained from the Sakarya University Educational and Research Hospital's Eye Clinic. Haemoglobin, URE, Glycated Haemoglobin, High-Density Lipoprotein,

Diabetes Duration, Low-Density Lipoprotein, Creatinin, Triglyceride, and Glucose are among the dataset's attributes. The classification accuracy of the Naive Bayes classifier was 89%. To improve the clarity of the proposed system performance more performance metric like precision, loss function, recall, area under the curve and f-score should be used.

Chetoui et al (2018) proposed the use of new texture features, mainly Local Ternary Pattern (LTP) and Local Energy-based Shape Histogram (LESH) for DR classification. These techniques capture the local relationship between neighbouring pixels and features and are less sensitive to variation in illumination, colour, and noise. These features extracted from the retinal fundus images were used to learn signs of Haemorrhages, hard Exudates, and Micro-aneurysms (HEM) and differentiate between DR and non-DR. Support Vector Machine (SVM) was used to classify these features. Polynomial and RBF kernels were the best performing in the detection of DR. The proposed technique was only trained to classify Fundus images as (0) non-DR and (1) DR.

Sarwinda et al (2017) provided a full model of Local Binary Pattern (LBP) as a texture feature descriptor technique for DR detection. In this study, the feature selection method was Expectation Maximization-Principal Component Analysis (EM-PCA), and the classification technique was KNN. The LBP feature descriptor approach was used to extract magnitude, sign, and mean values. The STARE Diabetic Retinopathy database was used in this investigation, which contains 66 DR photos and 44 normal images with a resolution of 700 x 600 pixels. A combination of the LBP sign and magnitude value showed a better sensitivity of 98.48% than a

mixture of LBP mean value and sign, and the LBP magnitude and mean values with sensitivity of 97.5% and 97% respectively. A drawback of this study is that the obtained results were not benchmarked with related works that used the STARE database. Also the extracted LBP features were only tested on the KNN classifier. More classifier can be used for testing the efficiency of these extracted features to improve the model robustness.

An automatic Diabetic Retinopathy identification technique based on a bag of words approach was presented by (Islam et al 2017). Based on five public datasets: Messidor (Decencière et al, 2014), STARE (Hoover & Goldbaum, 2003), DIARETDB1 (Kauppi et al 2007), DIARETDB0(Kauppi et al 2006), and High-Resolution Fundus (HRF), this approach classifies diabetic retinopathy images into absence or presence DR. The feature extraction technique employed was the Speed up Robust Features (Bay et al, 2008). The retrieved extracted feature was assigned to multiple clusters using the K-means clustering algorithm. Visual words are represented by the cluster centres, and these words together make up the lexicon, or bag of words. Each image feature is quantised to the nearest word, resulting in a histogram with each bin representing the frequency of a word inside that bag of words. The data was classified using SVM. The proposed method had 94.4% accuracy, precision, recall, and a 94%-score. The DR photos were simply classed as normal or abnormal in this investigation; with no regard for the severity level of the DR. Table 1 gives a summary of the related works.

A new approach to the diagnosis of Age-related Macular Degeneration (AMD) and DR as proposed by Morales etal.(2017). The presentation of a new technique for

the diagnosis of AMD and DR was the objective of this method. Five experiments were developed and tested using the suggested procedure: separating DR from normal, AMD from normal, pathological from normal, DR from AMD, and the three different classes (AMD, DR, and Normal): The LBP was used as the feature descriptor technique. The study's most noteworthy conclusion is that the new approach can distinguish between groups based on an analysis of the retina's spatial texture, thereby removing the retinal lesion's previous segmentation. The findings suggest that employing LBP as a texture descriptor for fundus photos provides useful characteristics for detecting retinal illness. This work, however, only investigated the LBP without further searching for more texture descriptors.

A graph-based approach to classifying retinal images was suggested by Mangrulkar (2018). The retinal images were pre-processed to eliminate noise and remove irrelevant information. The Canny edge detector was then utilised to identify the edges of the items in the image. Using the kirsch template that defines the presence of an edge, the segmentation process was then performed. The Kirsch model is used for the retrieval of blood vessels from the retinal image. Together with the graph nodes extracted from the image, the Speed-Up Robust Features (SURF) features were extracted by finding the intersection points and the terminal ends. Using the graph-based method, classification was carried out, and the Artery Vein Ratio (AVR) was measured. The AVR ratio is a realistic measure to classify a diabetes-free or diabetes patient. The proposed process achieved an accuracy of 88%. Without considering a more advanced DR stage, this research only focused on the early phase identification of DR.

Arade and Patil (2017) conducted a comparative study of DR using the K-NN and Bayesian classifier. An automated image processing system that detects DR gradation is presented in this paper. Blood vessel segmentation was done using the kirsch process, as it was found that retinal photos effectively differentiated the blood vessels. Differentiated vessels were extracted using moment invariants, grey level features. The DR severity was identified along with K-NN and Bayesian classifier using a feed-forward neural network. To validate the results obtained with an ophthalmologist, it was indicated that the Bayesian classifier generates results comparable to the expert opinion than the K-NN classifier. The accuracy of the Bayesian classifier obtained is 74%, while the precision for K-NN is 66%. It is possible to expand this work and improve classification performance by training more classifiers or performing an ensemble. Table 2.2 gives a summary of the related works.

Table 2.2 Summary of Related Works

S/N	AUTHOR(S)	YEAR	STRENGTH	WEAKNESS/LIMITATION
1	Bilal etal.	2021	The pre-processing step enhances abnormality presence as well as segmentation	The model has high complexity as it cost more to create, train and deploy
2	Kalyani etal.	2021	Capsules are independent, hen multiple capsules agree; the probability of correct detection	The proposed model is slow, mainly due to the inner loop of the dynamic routing algorithm.

is much higher.

3	Tymchenko et al	2020	The main advantage of this strategy is that it enhances generalisation and reduces uncertainty by employing a network ensemble that has been trained on a large data set and fine-tuned on the target data set.	Shapley Addictive exPlanations (SHAP) was calculated for just a single network without considering the SHAP of the full ensemble, which could result to more precise hyper - parameter optimisation
4	Li et al	2019	The proposed technique was able to detect diabetic retinopathy at the five main stages.	The proposed technique was limited by the lack of images of lesions 3 and 4 in the training data set used in this investigation
5	Zeng et al	2019	This suggested method produced the diagnosis result for both left and right eye independently	The binocular models will have difficulty validating datasets that do not have feature paired fundus images
6	Kirange et al	2019	Early diagnosis of diabetic retinopathy for early treatment and prevention	One limitation of this study is that it concentrated on early-stage DR detection rather than considering the stage of DR proliferation
7	Costa et al	2018	Made use of weak information to detect	This study was limited to just the SURF feature. In addition,

			the presence or absence of DR disease.	images were classified into just absence or presence of DR without consideration of the DR stages.
8	Al-Hazaimeh et al	2018	Early diagnosis of diabetic retinopathy for early treatment and prevention	The method is limited to a small dataset size
9	Sudha and Karthikeyan	2018	The proposed technique was able to detect the presence of diabetic retinopathy	To improve the clarity of the proposed system performance more performance metric like precision, loss function, recall, area under the curve and f-score should be used.
10	Chetoui et al	2018	Proposed the use of new texture features, mainly Local Ternary Pattern (LTP) and Local Energy-based Shape Histogram (LESH) for DR classification.	The proposed technique was only trained to classify Fundus images as (0) non-DR and (1) DR.
11	Sarwinda et al	2017	The classification accuracy was improved using the EM-PCA feature selection	Results were not benchmarked with related works that used the STARE database. Also the extracted LBP features were only tested on the KNN classifier.

12	Islam et al	2017	Robust technique as classification was based on five diversified datasets.	The DR photos were simply classed as normal or abnormal in this investigation, with no regard for the severity level of the DR
13	Morales et al	2017	The findings suggest that employing LBP as a texture descriptor for fundus photos provides useful characteristics for detecting retinal illness.	Only investigated the LBP without further searching for more texture descriptors.
14	Mangrulkar	2017	To improve the system performance, the canny edge detection technique was utilised to identify the edges of the items in the DR image	This research only focused on the early phase identification of DR without considering a more advanced DR stage,
15	Arade and Patil	2017	To improve the suggested system performance, blood vessel segmentation was done using the kirsch process	The accuracy of the Bayesian model is 74%, while the precision for K-NN is 66%. This work can be expanded to improve classification performance.

2.6 Summary of Review

From the summary in Table 2.2, the weakness of the DR research by Kirange et al.(2019) and Islam etal.(2017) is that the research both focused on the DR early-stage binary classification (normal or abnormal), without regard for the severity level of the DR. This study will solve this weakness by considering the four severity stages of DR.   In this study, the issue of complexity (Bilal et al 2021) will be solved by the use of a single model instead of a mix of model. The proposed model is also computational efficient as it incorporates feature extraction and classification in a single framework.

CHAPTER THREE

3.0 RESEARCH METHODOLOGY

This chapter presents the techniques used to achieve the aim of this study. Figure 3.1 presents the proposed system flowchart.
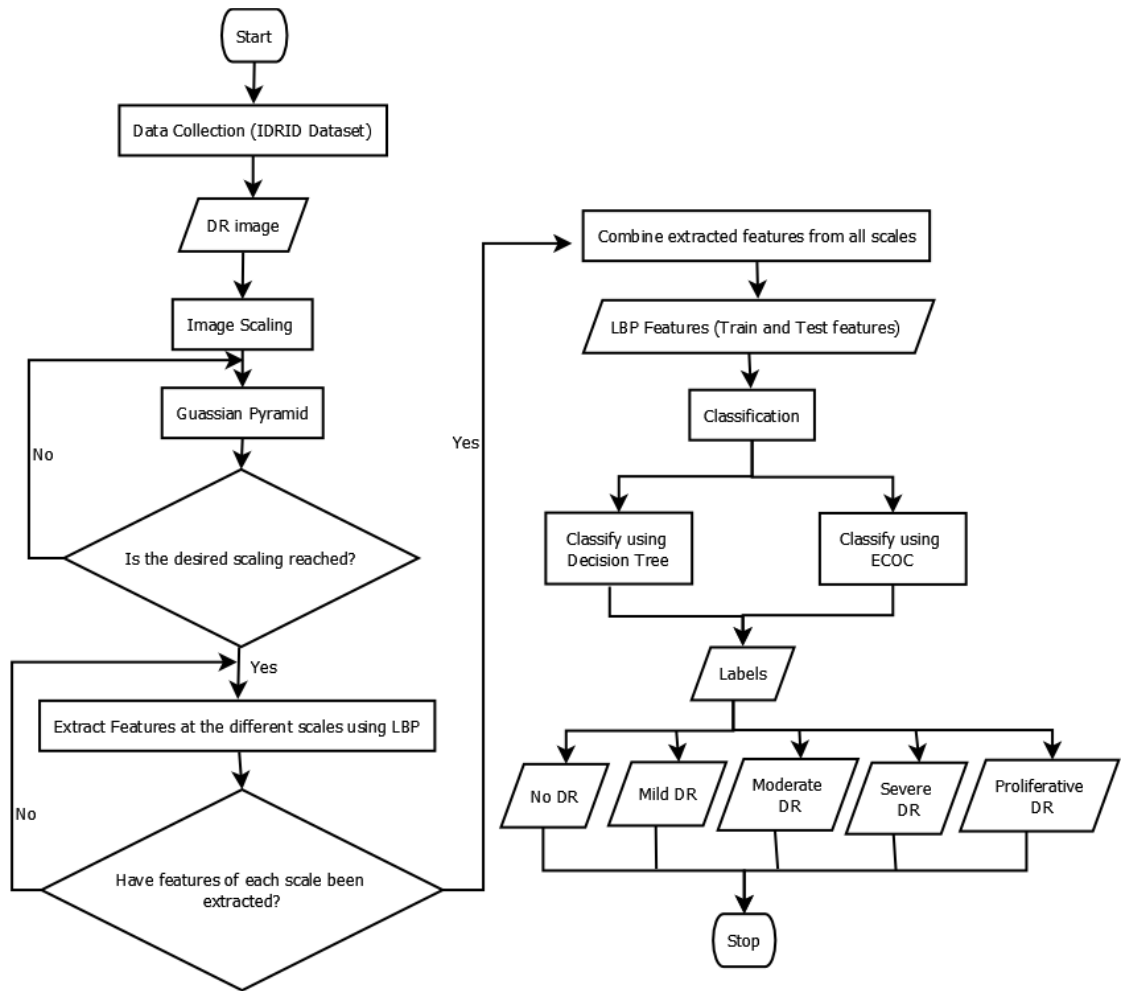
Figure 3.1 Proposed System

The flowchart shows the follow of the proposed system processes from the dataset collection stage down to the data labelling stage. Each of the steps and techniques shown in Figure 3.1 is explained in detail in this chapter.

3.1 Data Collection

A total of 516 DR fundus picture data were used in this study. These photographs were taken from the IDRiD dataset. The IDRiD dataset is a freely available retinal fundus image collection comprising 516 photos divided into two categories: DR and/or Diabetic Macular Edema (DME) retinal images and normal retinal images (without DR and/or DME) retinal images.

The medical specialists rated the entire set of 516 photos, which included a variety of DR and DME clinical situations. The dataset was separated into a training and testing set with 413 (80%) and 103 (20%) images, respectively, by preserving a good mixture of disease stratification.

For each image, the IDRiD dataset includes information on the disease severity of diabetic retinopathy, which ranges from 0 (no apparent DR) to 4 (severe DR), as well as the severity level of diabetic macular edema, which ranges from 0 (no DME) to 2 (severe DME). Figure 3.2, 3.3, 3.4, 3.5 and 3.6 are examples of IDRiD dataset showing the DR levels.

Figure 3. 2 No apparent DR (Label 0)

Figure 3. 3Mild Non proliferative DR (Label 1)

Figure 3. 4 Moderate Non proliferative DR

(Label 2)
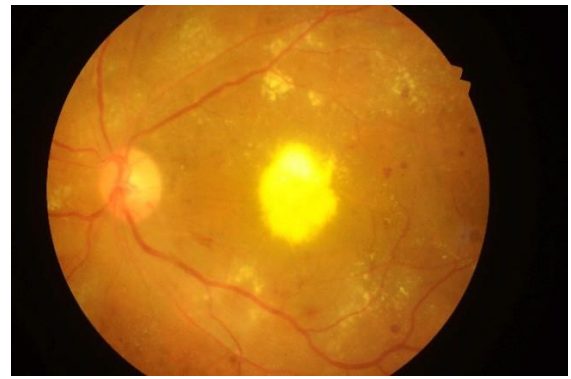
Figure 3. 5 Severe Non proliferative DR

(Label 3)

Figure 3. 6 Proliferative DR (Label 4)

This makes it ideal for creating and testing image analysis algorithms for diabetic retinopathy identification.

3.2 Image scaling

Image scaling is the process of changing the size of a digital image, either by making it smaller (down scaling) or larger (up scaling). Image scaling is used for a variety of purposes, such as resizing images for web or print, zooming in on specific parts of an image, or creating thumbnails. Image scaling is an essential pre-processing step in multi-scale feature extraction. It involves resizing the input image to different resolutions or scales to capture features at various levels of detail.

There are two main types of image scaling: interpolation and re-sampling. Interpolation is the process of adding new pixels to an image to increase its size,

while re-sampling involves reducing the size of an image by removing pixels. In this study the re-sampling method was used. Most filters are applied at a set scale to an image, although image features exist at all scales. Image Pyramid generates several image resolutions.

In the context of diabetic retinopathy diagnosis, the image scaling approach was used to analyze the retina at different scales to capture both local and global features. For example, small-scale features such as microaneurysms and haemorrhages may only be visible at high resolutions, while large-scale features such as optic disc and macula may be visible at lower resolutions.

The image Pyramid filtering approach was used to extract multi-scale features from the DR image while maintaining more edge details by creating several sizes of filtering windows. Each level of the image pyramid was subjected to Laplacian of Gaussian blob detection in order to identify features at various scales. The resulting feature maps at each level are then combined to produce a multi-scale feature map that captures features across multiple scales. The outcomes of filtering all layers of the image pyramid were merged to create multi-scale feature detection.

The following mathematical formula and explanation will give us a better grasp of how the image scaling approach functions.

Let's consider the process of sampling a continuous image function f at discrete spatial locations (pixels) to obtain a digital image. Let g be the digital image obtained by sampling f at a fixed sampling rate.

When the image is scaled by a factor of s, we are effectively changing the sampling rate of the image. Specifically, new sampling raters can be defined using equation 3.1:

$$rs = s \times r \qquad\qquad (3.1)$$

where r is the original sampling rate. The new image J(x',y') obtained by sampling f(x,y) at the new sampling rate is expressed in equation 3.2:

$$J(x',y') = f(x'/rs,\ y'/rs) \qquad\qquad (3.2)$$

where x' and y' are the coordinates of the pixel in the new image and rsis the new sampling rate. The expression x'/rs and y'/rs represents the scaling factor applied to the original coordinates to obtain the new coordinates in the scaled image.

To obtain a digital image from the continuous function J(x',y'), it needs to sampled at discrete spatial locations. This can be done using the same process as before, resulting in a digital image K(x',y') that represents the scaled version of the original image I(x,y).

The algorithm for the image scaling approach for image pre-processing is described in Table 3.1.

Table 3.1 Image Scaling Algorithm

Input: An image I of size (w, h) and a scaling factor s.
Output: A scaled image I' of size (sw, sh).
1. Start
2. Compute the new size of the image after scaling: sw = s * w, sh = s * h.
3. Create an empty image I' of size (sw, sh).
4. For each pixel (x', y') in the output image I':
a. Compute the corresponding pixel (x, y) in the input image I: x = x' / s, y = y' / s
b. If (x, y) is within the bounds of the input image I:
i.   Compute the colour value of the pixel at (x, y) using an interpolation method (e.g., nearest-neighbour, bilinear, bicubic).
ii.   Set the colour value of the pixel at (x', y') in the output image I' to the computed value.

> c. Otherwise, set the colour value of the pixel at (x', y') in the output image I' to a default value like black.
>
>   5. End

3.2.1 Image Pyramid.

A multi-scale depiction of an image is known as a "image pyramid." The use of an image pyramid allows us to locate items in photographs at various scales. In its original size, the original image is at the bottom of the pyramid (in terms of width and height). The image is shrunk (sub-sampled) and optionally smoothed at each subsequent layer (usually via Gaussian blurring). The image is gradually sub-sampled until a stopping condition is reached, which is usually a minimal size at which no more sub-sampling is required.

The purpose of an image pyramid is to provide a way to efficiently process images at different scales. By using an image pyramid, it is possible to analyse an image at multiple scales, allowing for the detection of features at different levels of detail.

There are two main types of image pyramids: Gaussian pyramids and Laplacian pyramids. Gaussian pyramids are created by repeatedly applying a Gaussian filter to the image and then down sampling it, while Laplacian pyramids are created by subtracting each image in a Gaussian pyramid from the next higher resolution image.

The Gaussian pyramid was utilised in this study. Subsequent photos in a Gaussian pyramid are scaled down and weighted down using a Gaussian average (Gaussian blur). A neighbourhood pixel on a lower level of the pyramid corresponds to each pixel carrying a local average. This form of accurate mathematical blurring is

commonly utilised as a pre-processing step in computer vision. When the edges of objects in a digital shot are blurred in this way, for example, they are easier to detect, allowing a computer to recognise them automatically.

To apply the Gaussian pyramid to this research problem, Firstly, the pyramid of the input retinal image was constructed. Each level of the pyramid represented a different scale of the image, with the top level representing the original image and the bottom level representing a highly down sampled version of the image.

Next, features from each level of the pyramid were extracted using the local binary patterns (LBP) feature extractor. Finally the features extracted from all levels of the pyramid were combined and used to train the decision tree and ECOC classifiers.

The DR photos were rescaled into three different scales using the image pyramid. The DR fundus image was initially scaled to 1440 by 960 pixels, then half that size, to 720 by 480 pixels. Finally, the final resolution is 360 by 240 pixels. The multi-scale features can be used to improve the DR classification results since they comprise discriminative properties from both the spectral dimension and their respective spatial scales. The algorithm for the Gaussian Pyramid method is described in Table 3.2.

Table 3.2 Algorithm for Gaussian Pyramid

Input: Original Image
Output: Images at different scale
1. Start
2. Load the original image at the highest resolution.
3. Initialize pyramid level
4. Apply a Gaussian filter to the image to remove high-frequency components and blur the image. The filter size used was 5x5.
5. Down-sample the image by a factor of 2 in both the horizontal and vertical

directions, which reduces the resolution of the image by half.

6. Repeat steps 3 and 4 for each level of the pyramid, until the desired number of levels is reached or until the image resolution is too low using a for loop.

7. Store each level of the pyramid in an array or list.

8. Return the scaled images

9. End

The resulting Gaussian pyramid is a series of images at different scales, with the original image at the highest resolution and the smallest image at the lowest resolution. Each level of the pyramid is obtained by applying a Gaussian filter to the previous level and then down-sampling it.

3.3 Feature Extraction

Feature extraction is a process of identifying and extracting relevant information or features from a raw data set. In the context of image processing and computer vision, feature extraction is a crucial step for recognising and understanding visual content.

The goal of feature extraction is to transform an image into a set of features that can be easily analysed and compared with other images. Features are usually represented as numerical values that capture certain properties of the image, such as texture, colour, shape, or edges. The algorithm for the feature extraction performed is given in Table 3.3.

Table 3.3 Algorithm for feature extraction

Input: A set of raw input data $X = \{x_1, x_2,..., x_n\}$.

Output: A set of features $F = \{f_1, f_2,..., f_m\}$.

1. Start
2. Define a feature extraction method (for example: LBP, SIFT, HOG) based on the nature of the input data and the task at hand.

49

3. For each input instance xi in X, apply the feature extraction method to obtain a set of features f_i.

4. Combine the features from all input instances into a feature matrix or vector representation that can be used for machine learning.

5. Optionally, normalise the features to improve their robustness and reduce redundancy (e.g., zero-mean normalisation, unit-length normalisation).

6. Return the set of features F.

7. End

Image features contain essential information such as points and edges that are vital for image analysis. It can be seen from Table 3.2 that there are several feature extraction methods that can be used to extract these image features. In this research, the Local BinaryPattern (LBP) was utilised for feature extraction. The LBP extractor is described further in the next section.

3.3.1 Local binary pattern (LBP)

The single-scale and the multi-scale features were extracted using the LBP descriptor. LBP was utilised for extracting features because it has been shown to extract extremely high-grade features, resulting in improved prediction performance LBP is a form of gray-level texture measure that uses an image's local contrast measure. LBP is an effective texture descriptor for images that sets a threshold for neighbouring pixels constructed on the current pixels' value. On a circle with a radius of R, there are C sampling sites in the neighbourhood and if given a pixel at (x_p, y_p). LBP can be expressed as shown in equation 3.3:

$$LBP_{C,R(x_p,y_p)} = \sum_{C=0}^{C-1} s(i_C - i_P)2^C \tag{3.3}$$

where i_c and i_p are, respectively, grey-level score of the central pixel and P surrounding pixels in the circle neighbourhood with a radius R, and function S(x) is

described in equation 3.4 as:

$$s(x) = \begin{cases} 1 & \text{if } x \geq 0 \\ 0 & \text{if } x < 0 \end{cases} \qquad (3.4)$$

The LBP operator used in this study is defined as follows:

1. Choose a pixel in an image and select a neighbourhood of surrounding pixels.

2. Compare the intensity value of each neighbour with the intensity value of the centre pixel.

3. If the neighbour's intensity value is greater than or equal to the centre pixel's intensity value, assign a value of 1 to that pixel in the binary pattern. Otherwise, assign a value of 0.

4. Concatenate the binary values of all the neighbours to form a binary pattern.

5. Convert the binary pattern to decimal and use it as a feature descriptor.

The algorithm for the local binary pattern feature descriptor is depicted in Table 3.4.

Table 3.4 Algorithm for computing the Local Binary Pattern (LBP) descriptor

Input: Greyscale image I of size M x N, radius r, and number of neighbours p.
Output: LBP image L of size M x N.

1. Start
2. For each pixel (x,y) in the image I, do the following:
3. Extract the circular neighbourhood with radius r centred at (x,y).
4. Compute the intensity difference between the centre pixel and each of its p neighbours using the formula:

$$d_i = I(x,y) - I(x_i - y_i) \text{ where}$$

(x_i, y_i) are the coordinates of the i-th neighbor.

5. Threshold the differences d_i using the center pixel intensity $I(x,y)$ as the threshold value: $s_i = 1$ if $d_i \geq 0$; 0 otherwise

6. Convert the binary sequence $s_1 \ldots s_p$ to decimal:

$$L(x,y) = \sum_{i=0}^{p-1} s_i \times 2^i$$

7. Repeat steps 2 to 6 for all pixels in the image to obtain the LBP image L.
8. Normalize the LBP image L by dividing each pixel value by the maximum LBP code value ($2^p - 1$) to obtain a normalized LBP image.

9. End

The resulting LBP image L is a two-dimensional matrix of integer values that represents the local texture patterns of the input image

LBP can be used to extract features from different scales and orientations of an image. The LBP texture descriptor was utilised in this study because it is easy to implement, and the computational cost is low. LBP is also invariant to monotonic illumination changes and LBP methodology combines architectural and statistical approaches, resulting in improved texture analysis performance.

3.4 Image Classification

Image classification is the process of categorizing an image into a predefined set of classes or categories based on its visual content. Machine Learning capability lies in its ability to generalise by correctly classifying unknown information based on models developed using the training dataset. In this study the two common steps taken for the image classification process are:

1. Model training: This step involves training a classification model using the selected features and a labelled dataset. The machine learning algorithms used for image classification in this research are the Error-Correcting Output Codes (ECOC), and the Decision Tree (DT).

2. Model evaluation: This step involves evaluating the performance of the trained model on a separate test dataset. The metrics used for the model evaluation include accuracy, precision, and recall. These metrics are discussed further in section 3.5.

3.4.1 Decision tree (DT)

A DT is a straightforward and widely used predictive modelling method. DT is a type of supervised learning in which data is repeatedly separated based on a specific parameter. The decision tree uses a tree-like structure to move from observations of an item (represented by the branches) to inferences about the item's target value (represented by the leaves). The DT algorithm can be used to tackle regression and classification problems. DT is simple to comprehend and view. Therefore, does not necessitate data standardisation or preparation, and it necessitates less labour. The decision to execute strategic splits has a big impact on the precision of a tree. Entropy, information gain and reduction invariance are techniques used in determining which attribute to the position at the root or the different levels of the tree.

The entropy of processed data is a measure of its randomness. The higher the entropy, the more difficult it is to draw any judgments from the information. A branch with entropy of zero, for example, is chosen as the root node, and further division is required for a branch with entropy greater than zero. In equation 3.5 entropy for a single attribute is expressed.

$$E(S) = \sum_{i=1}^{n} -p_i \log_2 p_i \qquad\qquad (3.5)$$

Where S denotes the present state, p_i is the likelihood of an event i of state S.

Information Gain (IG) is a statistical property that tests how well the training examples are segregated according to their target classification by a given attribute. In equation 3.6, information gain is expressed mathematically.

$$IG = Entropy(before) - \sum_{j=1}^{N} Entropy\ (j, after) \tag{3.6}$$

Where "before" refers to the dataset prior to the split, N refers to the number of subsets formed by the division, and (j,after)refers to subset jfollowing the division. Reduction invariant is a technique for solving regression problems. To choose the optimal split, this technique uses the usual variance formula. The split with the lowest variance is chosen as the criterion for dividing the population. The usual variance formula employed in this technique is stated in equation 3.7.

$$variance = \frac{\sum(X-\mu)^2}{n} \tag{3.7}$$

Where μ is the mean of the values and X is the actual value and n is the number of values.

Step by step approach for the decision tree model as used in this study is as follows:

1. Select the best attribute: The first step in building a decision tree is to select the best attribute to split the data on. This is usually done using a metric such as information gain or Gini impurity, which measures the reduction in entropy or impurity achieved by splitting the data on each attribute.

2. Create a node for the selected attribute: Once the best attribute has been selected, a node is created for it in the decision tree.

3. Partition the data: The data is then partitioned based on the values of the

selected attribute. Each partition corresponds to a branch in the decision tree, and the process is repeated recursively for each partition until a stopping criterion is met.

4. Assign a label: When a stopping criterion is met (e.g., all instances in a partition belong to the same class), a label is assigned to the corresponding leaf node in the decision tree.

5. Prune the tree: Once the decision tree has been constructed, it may be pruned to reduce over-fitting and improve its generalisation performance. This involves removing branches that do not contribute to the accuracy of the tree on the validation data.

6. Make predictions: To classify a new instance, the decision tree is traversed from the root node down to a leaf node, following the branch corresponding to the value of the selected attribute for the instance.

Decision trees have several advantages, including their interpretability, flexibility, and ability to handle both categorical and continuous data. The algorithm for the decision tree classification is depicted in Table 3.5.

Table 3.5 Algorithm for the Decision Tree Classifier Model

Input: A training dataset $D = \{(x_1, y_1), (x_2, y_2),..., (x_n, y_n)\}$, where x_i is a feature vector and y_i is the corresponding class label.
Output: A decision tree classifier.
1. Start
2. If all instances in D belong to the same class, create a leaf node with the class label and return it.
3. Otherwise, select the best attribute to split the data using a metric such as information gain or Gini impurity.

4. Create a new decision node for the selected attribute and its possible values.

5. Partition the data into subsets based on the selected attribute.

6. For each subset, repeat steps 2-5 recursively until a stopping criterion is met (e.g., maximum tree depth, minimum number of instances per leaf node, etc.).

7. Once the tree is constructed, prune it to reduce over-fitting and improve its generalisation performance.

8. Return the decision tree classifier.

9. End

To classify a new instance x, the decision tree is traversed from the root node down to a leaf node, following the branch corresponding to the value of the selected attribute for the instance. The class label of the leaf node is then assigned as the predicted class label for x.

3.4.2 Error-correcting output codes (ECOC)

Support Vector Machine (SVM) and logistic regression are examples of machine learning methods for binary classification issues. As a result, these binary techniques for multiclass classification issues either need to be upgraded or not used at all. The ECOC technique is a tool that allows a multiclass classification problem to be understood as a series of binary problems, allowing native binary classification models to be used directly. For each class, the ECOC allows for the encoding of an endless number of binary classification problems. Depending on the implementation, ECOC designs are independent of the classifier. In addition, ECOC has error-correcting features and has demonstrated that the bias and variance of the learning process can be reduced.

The ECOC architecture has two fundamental processes: coding and decoding. The

56

creation of a code matrix$\in \{-1, 0, 1\}^{c \times n}$ with c rows and n columns, where c and n signify the number of classes and dichotomizers, respectively, is the key to the coding process. The code word C_i for the ith class (i = 1, 2,..., c) appears in the ith row of M. In the meantime, each column of M reflects the dichotomizer's partition of classes. When training the dichotomizers, classes coded with 1 and -1 are regarded as positives and negatives, accordingly, whereas classes coded with 0 are omitted from the training set. The outputs of these n trained dichotomizers for the test sample are given as a vector $V = \{v_1, v_2,..., v_n\}$ in the decoding process and compared with the codeword of each class to find the closest one to determine the test sample's class label. In equation 3.8, the distance between the vector V and each codeword C_i is calculated.

$$D(V,C_i) = \frac{1}{2}\sum_{j=1}^{n} L(V(j).C_i(j)) \tag{3.8}$$

Where L(.) signifies the loss function which is reliant on the type of dichotomizer.

The basic idea of ECOC is to use a set of predefined codes to represent each class, and train a binary classifier for each bit position in the code.

Table 3. 6 Algorithm for Implementing Error-Correcting Output Codes (ECOC) for Multiclass Classification

Input: A training dataset $D = \{(x_1, y_1), (x_2, y_2),..., (x_n, y_n)\}$, where x_i is a feature vector and y_i is a multiclass label.

Output: A multiclass classifier.

1. Start
2. Define a set of k code matrices $C_1, C_2,..., C_k$ where each matrix represents a binary classification problem.
3. For each code matrix C_j, assign a unique binary label to each class in the training set using the code matrix.
4. Train a binary classifier for each bit position in each code matrix using the

corresponding binary labels.

5. For each test instance x, apply each binary classifier to obtain a set of binary outputs.

6. For each binary output, use the corresponding code matrix to map the binary output back to a multiclass label.

7. Combine the multiclass labels from all binary classifiers using a voting scheme (e.g., majority voting) to make a final prediction.

8. End

From the algorithm in Table 3.6 it that can be seen that step 4 requires training a binary classifier. A more detailed algorithm for training a binary classifier is depicted in Table 3.7.

Table 3.7 Algorithm for training a binary classifier using ECOC

Input: A binary code matrix C, where each row represents a unique binary label for a class.
Output: A binary classifier.

1. Start

2. For each row cof C, create a new training set D_c by assigning a positive label to instances with the corresponding bit set to 1, and a negative label to instances with the bit set to 0.

3. Train a binary classifier using the training set $D_c$and a chosen algorithm which is the Support Vector Machine.

4. Repeat steps 2-3 for all rows of C to obtain a set of binary classifiers.

5. Return the set of binary classifiers.

6. End

3.5 Performance Metrics

1. **Accuracy:** Accuracy is measured by the percentage of correctly classified instances. Accuracy is simply the number of correct estimates divided by total number of forecasts. In equation 3.7, the precise formulation is given:

58

$$\text{Accuracy} = \frac{TP + TN}{TP + TN + FP + FN} \qquad (3.9)$$

2. **Recall:** It is also recognised as sensitivity, and it is a measure that counts the number of correct positive predictions made out of all possible positive predictions. The formula in equation 3.8 is used to calculate recall.

$$\text{Recall} = \frac{TP}{TP + FN} \qquad (3.10)$$

3. **Precision**: is a measurement that counts the number of correct positive forecasts made. It is calculated by dividing the total number of true positives and false positives by the number of true positive elements. It is calculated using the formula in equation 3.9.

$$\text{Precision} = \frac{TP}{TP + FP} \qquad (3.11)$$

where TP is True Positives, TN is True Negatives, FN is False Negatives and Fp is False Positives.

4. **F1-Score:** F1-score is the harmonic mean of precision and recall, given by the formula:

$$\text{F1-score} = 2 * (\text{precision} * \text{recall}) / (\text{precision} + \text{recall}) \qquad 3.12$$

F1-score ranges from 0 to 1, where a higher score indicates better performance. It is particularly useful when the classes are imbalanced, as it balances the trade-off between precision and recall.

CHAPTER FOUR

4.0   RESULTS AND DISCUSSION

4.1 Results

4.1.1 DR Severity Grading Result

In this research, two types of experiments were conducted. Firstly, the image features were extracted on fixed scale. This single fixed scale image features were fed to the ECOC and DT classifier for the DR grading. Secondly, the DR images were scaled into three scales using the image pyramid method. The first scale was 1440 by 960, this scale was reduced by half to get the second image. Then, the third scale was obtained by reducing the second image by half. The features of these three images of different scales were extracted using the LBP extractor. After extraction these features were concatenated horizontally to form the multi-scale features. The multi-scale features were then supplied to the DT and SVM classification models for DR severity grading. The results of the different experimentations are shown in Table 4.1.

Table 4.1 DR Severity Grading Result

Method	Accuracy	Precision	Recall	F1-Score
Single scale +ECOC	52.88	45.06	52.88	48.16
Multi-scale +ECOC	65.05	48.31	64.66	55.10
Single scale + DT	54.80	56.68	54.80	50.62

| Multi-scale + DT | 66.35 | 50.01 | 66.35 | 55.40 |

Detailed explanation of the results shown in Table 4.1 is presented in the discussion section of this chapter. Figure 4.1is a coloured pattern bar chart representing the DR severity grading results for both the multi-scale and single-scaled models presented in Table 4.1.

DR Severity Grading Result

F1-Score ▨ Recall ▨ Precision ▨ Accuracy ▨
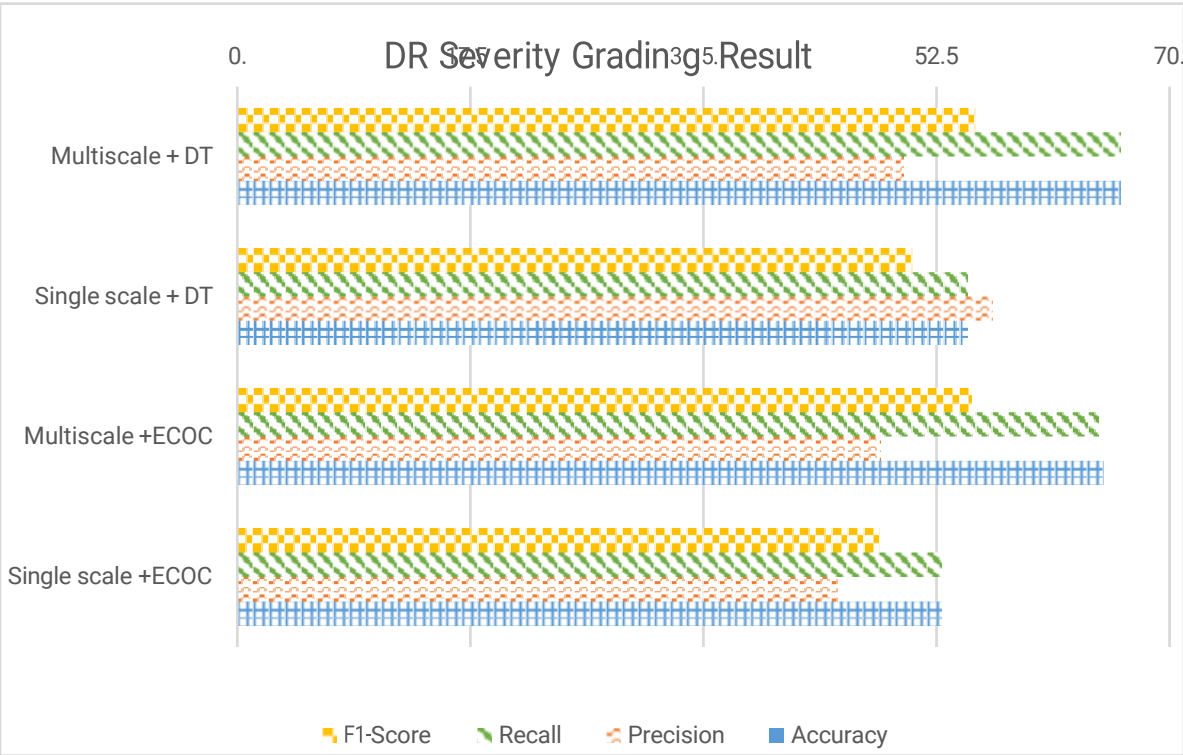
Figure 4. 1 Classification Result for ECOC and DT

4.1.2 Comparison with Existing Works

The best result from Table 4.1 was compared to the results of different

existing approaches in order to evaluate the performance of the proposed method.

The comparative result is shown in Table 4.2.

Table 4. 2 Comparison with the reported results on the IDRiD leaderboard

Method	ACCURACY (%)
Proposed Multi-scale features	66.35
VRT (Porwal et al 2020)	59.22
Mammoth (Porwal et al 2020)	54.37
HarangiM1 (Porwal et al 2020)	55.34
AVSASVA (Porwal et al 2020)	55.34
Harangi M2 (Porwal et al 2020)	47.57

The clustered column chart in Figure 4.2 compares the results of the proposed

method's accuracy performance metric against those of existing models, which

are reported in Table 4.2.
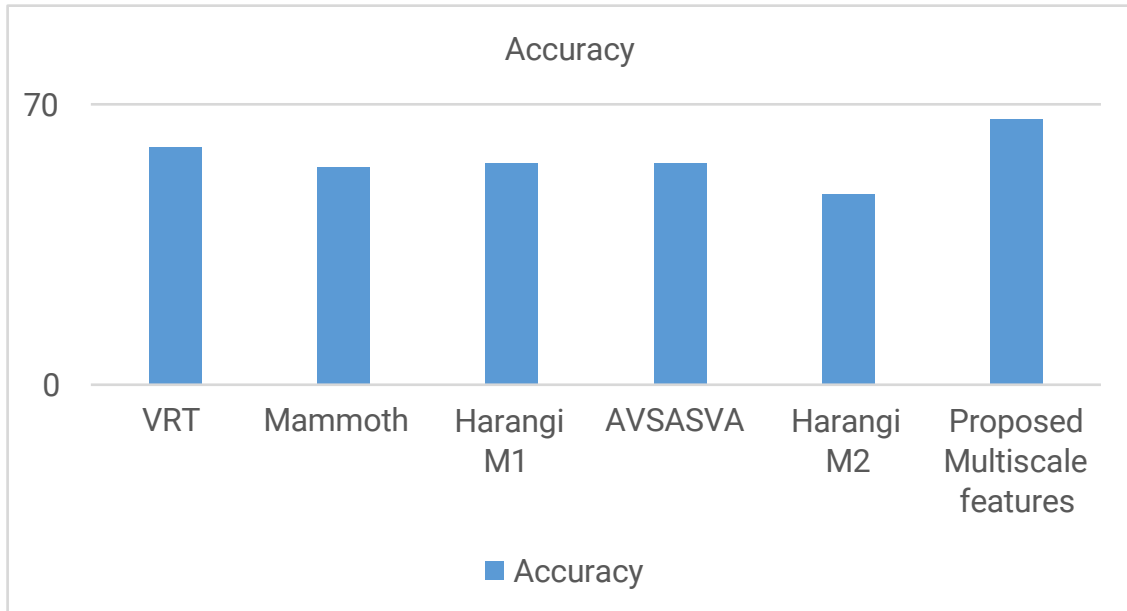
Figure 4. 2 Comparative results with existing methods

The discussion portion of this chapter provides a thorough explanation of the findings displayed in Table 4.2.

4.2 Discussion

4.2.1 DR Severity Grading

From Table 4.1, it can be inferred that all the extracted features produced a good accuracy value. However, the multi-scale features produced the highest classification accuracy with a value of 65.05% as compared to the single-scale features with a classification accuracy of 52.88% for ECOC model classification. Based on the precision metric for ECOC, the multi-scale features produced a slightly higher precision value of 48.31% than the single-scale features with 45.06% precision.

Looking at the obtained recall values for ECOC, the multi-scale features have a high recall value of 64.66%, which shows that the number of correct positive predictions

made from all the positive predictions is better than the positive prediction made by the single-scale features a recall of 52.88%.

Evaluating from the F1-score perspective for ECOC, the multi-scale features also produced the best F1-Score of 55.10%.

Comparing the single and multi-scale features based on the results obtained by the DT classification model, the single scale had lower accuracy, recall and f1-score of 54.80%, 54.80% and 50.40%, respectively, than multi-scale features with an accuracy of 66.35%, recall of 66.35% and f1-score of 55.40%. However, the quality of a positive prediction made by the DT model using single scale features was higher with a precision of 56.68 than when multi-scale features were used with a precision of 50.01%

From the accuracy, recall, precision, and f1-Score obtained, it can be concluded that the multi-scale features are more appropriate for a DR severity grading than the single-scale features.

4.2.2 Comparison with Existing Works

Table 4.2 shows the results of the proposed method and other challenge participation methods on the IDRiD challenge dataset. The proposed model was trained with only the data in the Sub-challenge 2 (image-level supervision). It is observed that multi-scale feature model achieves an accuracy of 66.35%, which is higher than the results by five teams in the leaderboard, with a relative 7.0% improvement on the accuracy. Lastly, it is worth noting that the proposed model was trained using only the data in Sub-challenge 2 in the IDRiD dataset, while others

may use model ensembles or other supervision provided in other Sub-challenges.

CHAPTER FIVE

5.0   CONCLUSION AND RECOMMENDATION

5.1 Conclusion

In conclusion, this study was able to execute DR severity rating more reliably than previous DR detection research. This is owing to the system's capacity to extract DR traits at various scales. From this study, it can be concluded that applying the multi-scale features improves the performance of classification models.. The first objective of identifying the challenges of existing diabetic retinopathy images detection and classification techniques were accomplished by reviewing several related works. The identified challenges includes: loss of scale-dependent information due to fixed scale feature extraction.

The image pyramid model was utilised to scale the original DR images into three different scales and then the texture features of each of the scaled images were extracted using the local binary pattern feature descriptor. The extracted features for a single image at different scales were concatenated to form the multi-scale features. This generated multi-scale features is an accomplishment of the second objective. The multi-scale feature descriptor model was evaluated against the single-scale feature descriptor model and against related works on diabetic retinopathy classification which completed the third objective. The multi-scale feature descriptor had the best performance with an accuracy of 66.35%, precision of 50.01%, recall 66.35%, and f1-score of 55.40|%. On the other hand, the single scale feature descriptor had the least performance with an accuracy of 54.80%, precision of 56.68%, recall of 54.80% and f1-score of 50.62%. These findings show that the proposed multi-scale feature descriptor technique is beneficial in improving DR categorization.

5.2 Recommendation

The following recommendations and suggestions for future works are made:

1. Improve the accuracy of the proposed method: Although the proposed method outperforms existing state-of-the-art methods in terms of accuracy, there is still room for improvement. Further optimization of the feature extraction and classification algorithms could lead to improved accuracy in the diagnosis of diabetic retinopathy.

2. Incorporate deep learning techniques: Deep learning techniques, such as

convolutional neural networks (CNNs), have shown great promise in image recognition and classification tasks. The incorporation of deep learning techniques could potentially improve the accuracy of the proposed method.

3. Expand the dataset: The proposed method was evaluated on publicly available datasets, which may not fully capture the diversity of retinal images in real-world scenarios. The collection and annotation of a larger and more diverse dataset could lead to improved performance and generalisation of the proposed method.

4. Consider other severity levels of diabetic retinopathy: The proposed method focused on the diagnosis of the severity level of diabetic retinopathy based on the four-level grading system. Future works could consider the diagnosis of other severity levels, such as mild non-proliferative diabetic retinopathy and severe non-proliferative diabetic retinopathy.

5. Develop a user-friendly interface: The proposed system could be made more user-friendly by developing a graphical user interface (GUI) that allows ophthalmologists to easily interact with the system and interpret the results.

6. Conduct clinical trials: The proposed method could be further validated through clinical trials to evaluate its efficacy and feasibility in real-world scenarios. This could potentially lead to the adoption of the proposed system in clinical practice, thereby improving the diagnosis and management of diabetic retinopathy.

5.3 Contribution to Knowledge

This study contributed to knowledge by developing a multi-scale feature extraction

model which graded diabetic retinopathy severity level into different categories.

REFERENCES

Abramoff, M. D., Garvin, M. K., &Sonka, M. (2010). Retinal Imaging and Image Analysis. *IEEE Reviews in Biomedical Engineering*, 3, 169. https://doi.org/10.1109/RBME.2010.2084567

Ahmad, A., Mansoor, A., Mumtaz, R., Khan, M., & Mirza, S. H. (2014). Image Processing and Classification in Diabetics Retinopathy: A Review. *IEEE 5th European Workshop on Visual Information Processing (EUVIP)*, 1–6

Ahmadi, M., Sharifi, A., Hassantabar, S., &Enayati, S. (2021). QAIS-DSNN: Tumor Area Segmentation of MRI Image with Optimized Quantum Matched-Filter Technique and Deep Spiking Neural Network. *BioMed Research International*, 2021. https://doi.org/10.1155/2021/6653879

al Hazaimeh, O. M., Nahar, K. M. O., al Naami, B., &Gharaibeh, N. (2018). An effective image processing method for detection of diabetic retinopathy diseases from retinal fundus images. *International Journal of Signal and Imaging Systems Engineering*, 11(4), 206. https://doi.org/10.1504/ijsise.2018.10015063

al Sariera, T. M., Rangarajan, L., & Amarnath, R. (2019). Detection and classification of hard exudates in retinal images. *Journal of Intelligent & Fuzzy Systems*, 38(2), 1943–1949. https://doi.org/10.3233/jifs-190492

Al-Rawi, M., Qutaishat, M., &Arrar, M. (2007). An improved matched filter for blood vessel detection of digital retinal images. *Computers in Biology and Medicine*, 37(2), 262–267. https://doi.org/10.1016/j.compbiomed.2006.03.003

Alsagheer, R. H. A., Alharan, A. F. H., & Al-haboobi, A. S. A. (2017). Popular Decision Tree Algorithms of Data Mining Techniques : A Review. *International Journal of Computer Science and Mobile Computing*, 6(6), 133–142.

Amin, J., Sharif, M., & Yasmin, M. (2016). A Review on Recent Developments for Detection of Diabetic Retinopathy. *Scientifica*, 2016 https://doi.org/10.1155/2016/6838976

Arade, S. P., & Patil, J. K. (2017). Comparative Study of Diabetic Retinopathy Using K-NN and Bayesian Classifier. *International Journal of Innovations in Engineering Research and Technology*, 4(5), 55–61.

Arcadu, F., Benmansour, F., Maunz, A., Willis, J., Haskova, Z., &Prunotto, M. (2019). Deep learning algorithm predicts diabetic retinopathy progression in individual patients. *Npj Digital Medicine*, 2(1). https://doi.org/10.1038/s41746-019-0172-3

Armano, G., Chira, C., &Hatami, N. (2013). Error-Correcting Output Codes for Multi-Label

Text Categorization. *International Journal of Refrigeration,* 12(4), 26–37.

Auccahuasi, W., Flores, E., Sernaque, F., Cueva, J., Diaz, M., &Oré, E. (2020). Recognition of hard exudates using Deep Learning. *Procedia Computer Science,* 167, 2343–2353. https://doi.org/10.1016/j.procs.2020.03.287

Banu, R., Arun, V., Shankaraiah, N., & Shyam, V. (2016). Meta-cognitive neural network method for classification of diabetic retinal images. *Proceedings - 2016 2nd International Conference on Cognitive Computing and Information Processing, CCIP 2016.* https://doi.org/10.1109/CCIP.2016.7802860

Basar, S., Ali, M., Ochoa-Ruiz, G., Zareei, M., Waheed, A., & Adnan, A. (2020). Unsupervised color image segmentation: A case of RGB histogram based K-means clustering initialization. *PLOS ONE,* 15(10), e0240015. https://doi.org/10.1371/JOURNAL.PONE.0240015

Basit, A., & Egerton, S. J. (2013). Bio-medical imaging: Localization of main structures in retinal fundus images. *IOP Conference Series: Materials Science and Engineering,* 51(1). https://doi.org/10.1088/1757-899X/51/1/012009

Baug, A., Choudhury, N. R., Ghosh, R., Dalai, S., & Chatterjee, B. (2017). Identification of single and multiple partial discharge sources by optical method using mathematical morphology aided sparse representation classifier. *IEEE Transactions on Dielectrics and Electrical Insulation,* 24(6), 3703–3712. https://doi.org/10.1109/TDEI.2017.006398

Bay, H., Ess, A., Tuytelaars, T., & van Gool, L. (2008). Speeded-Up Robust Features (SURF). *Computer Vision and Image Understanding,* 110(3), 346–359. https://doi.org/10.1016/j.cviu.2007.09.014

Benger, M., Williams, O., Siddiqui, J., &Sztriha, L. (2020). Intracerebral haemorrhage and COVID-19: Clinical characteristics from a case series. *Brain, Behavior, and Immunity,* 88, 940–944. https://doi.org/10.1016/j.bbi.2020.06.005

Bilal, A., Sun, G., Li, Y., Mazhar, S., & Khan, A. Q. (2021). Diabetic Retinopathy Detection and Classification Using Mixed Models for a Disease Grading Database. *IEEE Access,* 9, 23544–23553. https://doi.org/10.1109/ACCESS.2021.3056186

Bus, S. A., Lavery, L. A., Monteiro-Soares, M., Rasmussen, A., Raspovic, A., Sacco, I. C. N., & van Netten, J. J. (2020). Guidelines on the prevention of foot ulcers in persons with diabetes (IWGDF 2019 update). *Diabetes/Metabolism Research and Reviews,* 36Suppl1(S1). https://doi.org/10.1002/DMRR.3269

Çeliktutan, O., Ulukaya, S., &Sankur, B. (2013). A comparative study of face landmarking techniques. *Eurasip Journal on Image and Video Processing,* 2013(1), 1–27.

https://doi.org/10.1186/1687-5281-2013-13

Chaudhuri, S., Chatterjee, S., Katz, N., Nelson, M., &Goldbaum, M. (1989). Detection of blood vessels in retinal images using two-dimensional matched filters. IEEE Transactions on Medical Imaging 8(3), 263–269. https://doi.org/10.1109/42.34715

Chen, L., Messinger, J. D., Sloan, K. R., Swain, T. A., Sugiura, Y., Yannuzzi, L. A., Curcio, C. A., & Freund, K. B. (2020). Nonexudative Macular Neovascularization Supporting Outer Retina in Age-Related Macular Degeneration: A Clinicopathologic Correlation. Ophthalmology 127(7), 931–947. https://doi.org/10.1016/j.ophtha.2020.01.040

Chen, T., Trinder, J. C., &Niu, R. (2017). Object-oriented landslide mapping using ZY-3 satellite imagery, random forest and mathematical morphology, for the Three-Gorges Reservoir, China. Remote Sensing 9(4). https://doi.org/10.3390/rs9040333

Chetoui, M., Akhloufi, M., &Kardouchi, M. (2018). Diabetic Retinopathy Detection Using Machine Learning and Texture Features. 2018 IEEE Canadian Conference on Electrical & Computer Engineering (CCECE) 178–181. https://doi.org/10.1109/TENSYMP50017.2020.9230600

Cholaquidis, A., &Fraiman, R. (2018). Semisupervised learning Semisupervised learning When and why it works Houdacton September https://doi.org/10.1007/s11749-019-00690-2

Choudhary, B. K., Kumar Choudhary, B., Kumar, N., And, S., & Shanker, P. (2012). Pyramid Method In Image Processing Study Of Nonclassical Properties View Project Pyramid Method Image Processing Journal of Information Systems and Communication 3(1). http://www.bioinfo.in/contents.php?id=45

Costa, P., Galdran, A., Smailagic, A., &Campilho, A. (2018). A Weakly-Supervised Framework for Interpretable Diabetic Retinopathy Detection on Retinal Images. IEEE Access, 6, 18747–18758. https://doi.org/10.1109/ACCESS.2018.2816003

Cree, M. J., Cornforth, D. J., & Jelinek, H. F. (2005). Vessel segmentation and tracking using a two-dimensional model. Image and Vision Computing New Zealand http://citeseerx.ist.psu.edu/viewdoc/download?doi=10.1.1.124.8341&rep=rep1&type=pdf

Decencière, E., Zhang, X., Cazuguel, G., Laÿ, B., Cochener, B., Trone, C., Gain, P., Ordóñez-Varela, J. R., Massin, P., Erginay, A., Charton, B., & Klein, J. C. (2014). Feedback on a publicly distributed image database: The Messidor database. Image Analysis and Stereology 33(3), 231–234. https://doi.org/10.5566/IAS.1155

Dietterich, T. G., &Bakiri, G. (1995). Solving Multiclass Learning Problems via Error-

Correcting Output Codes. In *Journal of Artificial Intelligence Research* (Vol. 2).

Dutta, S., Manideep, B. C. S., Basha, S. M., Caytiles, R. D., & Iyengar, N. C. S. N. (2018). Classification of diabetic retinopathy images by using deep learning models. *International Journal of Grid and Distributed Computing,* 11(1), 89–106. https://doi.org/10.14257/ijgdc.2018.11.1.09

Escalera, S., Pujol, O., &Radeva, P. (2010). Error-Correcting Ouput Codes Library. *Journal of Machine Learning Research,* 11, 661–664. https://doi.org/10.5555/1756006

Fraz, M. M., Barman, S. A., Remagnino, P., Hoppe, A., Basit, A., Uyyanonvara, B., Rudnicka, A. R., & Owen, C. G. (2012). An approach to localize the retinal blood vessels using bit planes and centerline detection. *Computer Methods and Programs in Biomedicine,* 108(2), 600–616. https://doi.org/10.1016/j.cmpb.2011.08.009

Ganesan, K., Martis, R. J., Acharya, U. R., Chua, C. K., Min, L. C., Ng, E. Y. K., & Laude, A. (2014). Computer-aided diabetic retinopathy detection using trace transforms on digital fundus images. *Medical and Biological Engineering and Computing,* 52(8), 663–672. https://doi.org/10.1007/s11517-014-1167-5

Ganesan, K., Naik, G., Adapa, D., Raj, A. N. J., Alisetti, S. N., & Zhuang, Z. (2020). A supervised blood vessel segmentation technique for digital Fundus images using Zernike Moment based features. *PLoS ONE,* 15(3). https://doi.org/10.1371/journal.pone.0229831

George, M., &Zwiggelaar, R. (2019). Comparative study on local binary patterns for mammographic density and risk scoring †. *Journal of Imaging,* 5(2). https://doi.org/10.3390/jimaging5020024

Gulshan, V., Peng, L., Coram, M., Stumpe, M. C., Wu, D., Narayanaswamy, A., Venugopalan, S., Widner, K., Madams, T., Cuadros, J., Kim, R., Raman, R., Nelson, P. C., Mega, J. L., & Webster, D. R. (2016). Development and validation of a deep learning algorithm for detection of diabetic retinopathy in retinal fundus photographs. *JAMA - Journal of the American Medical Association,* 316(22), 2402–2410. https://doi.org/10.1001/jama.2016.17216

Guo, S., Wang, K., Kang, H., Liu, T., Gao, Y., & Li, T. (2020). Bin loss for hard exudates segmentation in fundus images. *Neurocomputing,* 392, 314–324. https://doi.org/10.1016/j.neucom.2018.10.103

Hammoudeh, A. (2018). A Concise Introduction to Reinforcement Learning. *Iteration Journal of Innovation in Engineering and Technology (IJIET) February.* https://doi.org/10.13140/RG.2.2.31027.53285

Haoran, L., Huiyuan, F., Xiaojun, H., & Liang, L. (2019). ESNET: Edge-based segmentation Network for Real-Time Semantic Segmentation in Traffic Scenes. *IEEE International Conference on Image Processing (ICIP) Proceedings*, 1855–1860.

Heikkilä, M., Pietikäinen, M., & Schmid, C. (2009). Description of interest regions with local binary patterns. *Pattern Recognition*, 42(3), 425–436. https://doi.org/10.1016/j.patcog.2008.08.014

Hoover, A. (2000). Locating blood vessels in retinal images by piecewise threshold probing of a matched filter response. *IEEE Transactions on Medical Imaging*, 19(3), 203–210. https://doi.org/10.1109/42.845178

Hoover, A., &Goldbaum, M. (2003). Locating the optic nerve in a retinal image using the fuzzy convergence of the blood vessels. *IEEE Transactions on Medical Imaging*, 22(8), 951–958. https://doi.org/10.1109/TMI.2003.815900

Huang, C., Zong, Y., Ding, Y., Luo, X., Clawson, K., & Peng, Y. (2021). A new deep learning approach for the retinal hard exudates detection based on superpixel multi-feature extraction and patch-based CNN. *Neurocomputing*, 452, 521–533. https://doi.org/10.1016/j.neucom.2020.07.145

Huang, D., Shan, C., Ardabilian, M., Wang, Y., & Chen, L. (2011). Local binary patterns and its application to facial image analysis: A survey. *IEEE Transactions on Systems, Man and Cybernetics Part C (Applications and Reviews)*, 41(6), 765–781. https://doi.org/10.1109/TSMCC.2011.2118750

Humeau-Heurtier, A. (2019). Texture feature extraction methods: A survey. *IEEE Access*, 7, 8975–9000. https://doi.org/10.1109/ACCESS.2018.2890743

Islam, M., Dinh, A. v., & Wahid, K. A. (2017). Automated Diabetic Retinopathy Detection Using Bag of Words Approach. *Journal of Biomedical Science and Engineering*, 10(05), 86–96. https://doi.org/10.4236/jbise.2017.105b010

Jia, D., & Zhuang, X. (2021). Learning-based algorithms for vessel tracking: A review. In *Computerized Medical Imaging and Graphics* (Vol. 89). Elsevier Ltd. https://doi.org/10.1016/j.compmedimag.2020.101840

Kalyani, G., Janakiramaiah, B., Karuna, A., & Prasad, L. V. N. (2021). Diabetic retinopathy detection and classification using capsule networks. *Complex & Intelligent Systems*. https://doi.org/10.1007/s40747-021-00318-9

Kande, G. B., Subbaiah, P. V., &Savithri, T. S. (2010). Unsupervised fuzzy based vessel segmentation in pathological digital fundus images. *Journal of Medical Systems*, 34(5), 849–858. https://doi.org/10.1007/s10916-009-9299-0

Kato, A., & Nakagawa, S. (2020). Detection of deep low-frequency earthquakes in the Nankai subduction zone over 11 years using a matched filter technique. *Earth Planets and Space*, 72(1). https://doi.org/10.1186/s40623-020-01257-4

Kauppi, T., Kalesnykiene, V., Kamarainen, J. K., Lensu, L., Sorri, I., Raninen, A., Voutilainen, R., Pietilä, J., Kälviäinen, H., &Uusitalo, H. (2007). The DIARETDB1 diabetic retinopathy database and evaluation protocol. *BMVC 2007 - Proceedings of the British Machine Vision Conference 2007*. https://doi.org/10.5244/C.21.15

Kauppi, T., Kalesnykiene, V., Kamarainen, J.-K., Lensu, L., Sorri, I., Uusitalo, H., Kälviäinen, H., &Pietilä, J. (2006). DIARETDB0: Evaluation Database and Methodology for Diabetic Retinopathy Algorithms. *Proceedings of the British Machine Vision Conference 2007*.

Kesidou, D., da Costa Martins, P. A., de Windt, L. J., Brittan, M., Beqqali, A., & Baker, A. H. (2020). Extracellular Vesicle miRNAs in the Promotion of Cardiac Neovascularisation. In *Frontiers in Physiology* (Vol. 11). Frontiers Media S.A. https://doi.org/10.3389/fphys.2020.579892

Khan, A., Garner, R., Rocca, M. La, Salehi, S., & Duncan, D. (2022). A Novel Threshold-Based Segmentation Method for Quantification of COVID-19 Lung Abnormalities. *Signal, Image and Video Processing 2022*, 1–8. https://doi.org/10.1007/S11760-022-02183-6

Kirange, D. K., Chaudhari, J. P., Rane, K. P., Bhagat, K. S., &Chaudhri, N. (2019). Diabetic retinopathy detection and grading using machine learning. *International Journal of Advanced Trends in Computer Science and Engineering*, 8(6), 3570–3576. https://doi.org/10.30534/ijatcse/2019/139862019

Kurilová, V., Goga, J., Oravec, M., Pavlovičová, J., &Kajan, S. (2021). Support vector machine and deep-learning object detection for localisation of hard exudates. *Scientific Reports*, 11(1). https://doi.org/10.1038/s41598-021-95519-0

Li, G., Xiao, X., Tang, J. T., Li, J., Zhu, H. J., Zhou, C., & Yan, F. B. (2017). Near-source noise suppression of AMT by compressive sensing and mathematical morphology filtering. *Applied Geophysics*, 14(4), 581–589. https://doi.org/10.1007/s11770-017-0645-6

Li, T., & Song, J. (2007). Construction of Decision Trees based Entropy and Rough Sets under Tolerance Relation. *International Journal of Computational Intelligence Systems, October*. https://doi.org/10.2991/iske.2007.258

Li, Y. H., Yeh, N. N., Chen, S. J., & Chung, Y. C. (2019). Computer-Assisted Diagnosis for Diabetic Retinopathy Based on Fundus Images Using Deep Convolutional Neural Network. *Mobile Information Systems*, 2019(1).

https://doi.org/10.1155/2019/6142839

Li, Z., Guo, C., Nie, D., Lin, D., Yi, Z., Chen, C., Xiang, Y., Xu, F., Jin, C., Zhang, X., Yang, Y., Zhang, K., Zhao, L., Zhang, P., Han, Y., Yun, D., Xiaohang, W., Yan, P., & Lin, H. (2020). Development and evaluation of a deep learning system for screening retinal hemorrhage based on ultra-widefield fundus images. *Translational Vision Science and Technology*, 9(2). https://doi.org/10.1167/tvst.9.2.3

Lin, L., Li, M., Huang, Y., Cheng, P., Xia, H., Wang, K., Yuan, J., & Tang, X. (2020). The SUSTech-SYSU dataset for automated exudate detection and diabetic retinopathy grading. *Scientific Data*, 7(1). https://doi.org/10.1038/s41597-020-00755-0

Liu, Q., Liu, H., Zhao, Y., & Liang, Y. (2022). Dual-Branch Network with Dual-Sampling Modulated Dice Loss for Hard Exudate Segmentation in Color Fundus Images. *IEEE Journal of Biomedical and Health Informatics*, 26(3), 1091–1102. https://doi.org/10.1109/JBHI.2021.3108169

Luo, J., Liu, J., Lin, J., & Wang, Z. (2020). A lightweight face detector by integrating the convolutional neural network with the image pyramid. *Pattern Recognition Letters*, 133, 180–187. https://doi.org/10.1016/j.patrec.2020.03.002

Ma, Y., Hao, H., Xie, J., Fu, H., Zhang, J., Yang, J., Wang, Z., Liu, J., Zheng, Y., & Zhao, Y. (2021). ROSE: A Retinal OCT-Angiography Vessel Segmentation Dataset and New Model. *IEEE Transactions on Medical Imaging* 40(3), 928–939. https://doi.org/10.1109/TMI.2020.3042802

Mangrulkar, R. S. (2018). Retinal image classification technique for diabetes identification. *Proceedings of 2017 International Conference on Intelligent Computing and Control, I2C2 2017, 2018-January*, 1–6. https://doi.org/10.1109/I2C2.2017.8321873

Manojkumar, S. B., U, S. F., Anandaraju, M. B., &Sheshadri, H. S. (2019). *Retinal Disease Detection Using BP Technique December 2018*

Mateen, M., Wen, J., Nasrullah, N., Sun, S., & Hayat, S. (2020). Exudate Detection for Diabetic Retinopathy Using Pretrained Convolutional Neural Networks. *Complexity 2020* https://doi.org/10.1155/2020/5801870

McGuire, B. A., Loomis, R. A., Burkhardt, A. M., Long Kelvin Lee, K., Shingledecker, C. N., Charnley, S. B., Cooke, I. R., Cordiner, M. A., Herbst, E., Kalenskii, S., Siebert, M. A., Willis, E. R., Xue, C., Remijan, A. J., & McCarthy, M. C. (2021). *Detection of two interstellar polycyclic aromatic hydrocarbons via spectral matched filtering* https://www.science.org

Mendonça, A. M., &Campilho, A. (2006). Segmentation of retinal blood vessels by

combining the detection of centerlines and morphological reconstruction. *IEEE Transactions on Medical Imaging*, 25(9), 1200–1213. https://doi.org/10.1109/TMI.2006.879955

Mohamed, A., El-Rafei, I., By, S., Salwa, P., El-Ramly, H., & Abdelhamid, L. S. (2017). *Retinal Image Analysis using Image Processing Techniques*.

Morales, S., Engan, K., Naranjo, V., &Colomer, A. (2017). Retinal Disease Screening Through Local Binary Patterns. *IEEE Journal of Biomedical and Health Informatics*, 21(1), 184–192. https://doi.org/10.1109/JBHI.2015.2490798

Nicholas, M. P., & Mysore, N. (2021). Corneal neovascularization. *Experimental Eye Research*, 202. https://doi.org/10.1016/j.exer.2020.108363

Niemeijer, M., van Ginneken, B., Staal, J., Suttorp-Schulten, M. S. A., &Abràmoff, M. D. (2005). Automatic detection of red lesions in digital color fundus photographs. *IEEE Transactions on Medical Imaging*, 24(5), 584–592. https://doi.org/10.1109/TMI.2005.843738

Oloumi, F., Rangayyan, R. M., & Ells, A. L. (2014). Digital image processing for ophthalmology: Detection and modeling of retinal vascular architecture. *Synthesis Lectures on Biomedical Engineering*, 49, 1–174. https://doi.org/10.2200/S00569ED1V01Y201402BME049

Pak, A., Ziyaden, A., Tukeshev, K., Jaxylykova, A., &Abdullina, D. (2020). Comparative analysis of deep learning methods of detection of diabetic retinopathy. *Cogent Engineering*, 7(1). https://doi.org/10.1080/23311916.2020.1805144

Pang, Y., Wang, T., Muhammad Anwer, R., Shahbaz Khan, F., & Shao, L. (2018). Efficient Featurized Image Pyramid Network for Single Shot Detector. *Computer Vision Foundation*, 7337–7344.

Paris, S., Hasinoff, S. W., & Kautz, J. (2015). Local Laplacian filters: Edge-aware image processing with a Laplacian pyramid. *Communications of the ACM*, 58(3), 81–91. https://doi.org/10.1145/2723694

Park, H. S., Byun, Y., Byeon, S. H., Kim, S. S., Kim, Y. J., & Lee, C. S. (2021). Retinal hemorrhage after sars-cov-2 vaccination. *Journal of Clinical Medicine*, 10(23). https://doi.org/10.3390/jcm10235705

Park, K. B., Choi, S. H., & Lee, J. Y. (2020). M-GAN: Retinal Blood Vessel Segmentation by Balancing Losses through Stacked Deep Fully Convolutional Networks. *IEEE Access*, 8, 146308–146322. https://doi.org/10.1109/ACCESS.2020.3015108

Patel, S. N., Klufas, M. A., Ryan, M. C., Jonas, K. E., Ostmo, S., Martinez-Castellanos, M.

A., Berrocal, A. M., Chiang, M. F., & Chan, R. V. P. (2015). Color fundus photography versus fluorescein angiography in identification of the macular center and zone in retinopathy of prematurity. *American Journal of Ophthalmology* 159(5), 950- 957.e2. https://doi.org/10.1016/j.ajo.2015.01.027

Porwal, P., Pachade, S., Kamble, R., Kokare, M., Deshmukh, G., Sahasrabuddhe, V., &Meriaudeau, F. (2018). Indian Diabetic Retinopathy Image Dataset (IDRiD): A Database for Diabetic Retinopathy Screening Research. *Data 2018, Vol. 3, Page 25*, 3(3), 25. https://doi.org/10.3390/DATA3030025

Porwal, P., Pachade, S., Kokare, M., Deshmukh, G., Son, J., Bae, W., Liu, L., Wang, J., Liu, X., Gao, L., Wu, T. B., Xiao, J., Wang, F., Yin, B., Wang, Y., Danala, G., He, L., Choi, Y. H., Lee, Y. C., … Mériaudeau, F. (2020). IDRiD: Diabetic Retinopathy – Segmentation and Grading Challenge. *Medical Image Analysis*, 59. https://doi.org/10.1016/j.media.2019.101561

Priyanka Mahendra Prasad, & Dr. H. G. Virani. (2017). Segmentation and Classification of Retinal Image Features. *International Journal of Engineering Research And*, V6(04). https://doi.org/10.17577/IJERTV6IS040554

Public Health England. (2016, September 13). *3.8 million people in England now have diabetes*. UK Health Security Agency Press Office.

Rahimy, E. (2018). Deep learning applications in ophthalmology. *Current Opinion in Ophthalmology*, 29(3), 254−260. https://doi.org/10.1097/ICU.0000000000000470

Rahman, M. M., Garcia, N., Loh, Y. S., Marks, D. C., Banakh, I., Jagadeesan, P., Cameron, N. R., Yung-Chih, C., Costa, M., Peter, K., Cleland, H., &Akbarzadeh, S. (2021). A platelet-derived hydrogel improves neovascularisation in full thickness wounds. *Acta Biomater*, 136, 199−209. https://doi.org/10.1016/j.actbio.2021.09.043

Rajalakshmi, R., Subashini, R., Anjana, R. M., & Mohan, V. (2018). Automated diabetic retinopathy detection in smartphone-based fundus photography using artificial intelligence. *Eye (Basingstoke)*, 32(6), 1138−1144. https://doi.org/10.1038/s41433 -018-0064-9

Ramlugun, G. S., Nagarajan, V. K., & Chakraborty, C. (2012). Small retinal vessels extraction towards proliferative diabetic retinopathy screening. *Expert Systems with Applications*, 39(1), 1141−1146. https://doi.org/10.1016/j.eswa.2011.07.115

Rodrigues, L. C., &Marengoni, M. (2017). Segmentation of optic disc and blood vessels in retinal images using wavelets, mathematical morphology and Hessian-based multi-scale filtering. *Biomedical Signal Processing and Control*, 36, 39−49. https://doi.org/10.1016/j.bspc.2017.03.014

Rokach, L., &Maimon, O. (2005). Decision Tree. In Data Mining and Knowledge DiscoveryHandbook(Issue August 2015, pp. 165–192). https://doi.org/10.1007/0- 387-25465-X

Romero-Aroca, P. (2015). Importance of telemedicine in diabetes care: Relationships between family physicians and ophthalmologists. World Journal of Diabetes, 6(8), 1005. https://doi.org/10.4239/wjd.v6.i8.1005

Sandhu, H. S., Eltanboly, A., Shalaby, A., Keynton, R. S., Schaal, S., & El-Baz, A. (2018). Automated diagnosis and grading of diabetic retinopathy using optical coherence tomography. Investigative Ophthalmology and Visual Science, 59(7), 3155–3160. https://doi.org/10.1167/iovs.17-23677

Sarki, R., Ahmed, K., Wang, H., & Zhang, Y. (2020). Automated detection of mild and multi-class diabetic eye diseases using deep learning. Health Information Science and Systems, 8(1), 1–9. https://doi.org/10.1007/s13755-020-00125-5

Saroj, S. K., Kumar, R., & Singh, N. P. (2020). Fréchet PDF based Matched Filter Approach for Retinal Blood Vessels Segmentation. Computer Methods and Programs in Biomedicine, 194. https://doi.org/10.1016/j.cmpb.2020.105490

Sarwinda, D., Bustamam, A., & Wibisono, A. (2017). A complete modelling of Local Binary Pattern for detection of diabetic retinopathy. Proceedings - 2017 1st International Conference on Informatics and Computational Sciences, ICICoS 2017, 2018- Janua, 7–10. https://doi.org/10.1109/ICICOS.2017.8276329

Sathya, R., & Abraham, A. (2013). Comparison of Supervised and Unsupervised Learning Algorithms for Pattern Classification. International Journal of Advanced Research in Artificial Intelligence, 2(2), 34–38.

Scherhag, U., Budhrani, D., Gomez-Barrero, M., & Busch, C. (2018). Detecting morphed face images using facial landmarks. Lecture Notes in Computer Science (including Subseries Lecture Notes in Artificial Intelligence and Lecture Notes in Bioinformatics), 10884 LNCS, 444–452. https://doi.org/10.1007/978-3-319-94211- 7_48

Selby, N. M., & Taal, M. W. (2020). An updated overview of diabetic nephropathy: Diagnosis, prognosis, treatment goals and latest guidelines. Diabetes, Obesity and Metabolism, 22(S1), 3–15. https://doi.org/10.1111/DOM.14007

Serwa, E. A. (2020). Studying the Potentiality of Using Digital Gaussian Pyramids in Multi-spectral Satellites Images Classification. Journal of the Indian Society of Remote Sensing. https://doi.org/10.1007/s12524-020-01173-w

Sharma, H., & Kumar, S. (2016). A Survey on Decision Tree Algorithms of Classification

in Data Mining. *International Journal of Science and Research (IJSR)* 5(4), 2094–2097.

Sharma, R. (2013). Use of Reinforcement Learning as a Challenge : A Review Use of Reinforcement Learning as a Challenge : A Review. *International Journal of Computer Applications,* 69(22), 28–34. https://doi.org/10.5120/12105-8332

Sinthanayothin, C., Boyce, J. F., Cook, H. L., & Williamson, T. H. (1999). Automated localisation of the optic disc, fovea, and retinal blood vessels from digital colour fundus images. *British Journal of Ophthalmology* 83(8), 902–910. https://doi.org/10.1136/bjo.83.8.902

Soares, J. V. B., Leandro, J. J. G., Cesar, R. M., Jelinek, H. F., & Cree, M. J. (2006). Retinal vessel segmentation using the 2-D Gabor wavelet and supervised classification. *IEEE Transactions on Medical Imaging* 25(9), 1214–1222. https://doi.org/10.1109/TMI.2006.879967

Somasundaram, S. K., & Alli, P. (2017). A Machine Learning Ensemble Classifier for Early Prediction of Diabetic Retinopathy. *Journal of Medical Systems,* 41(12). https://doi.org/10.1007/s10916-017-0853-x

Sopharak, A., Dailey, M. N., Uyyanonvara, B., Barman, S., Williamson, T., Nwe, K. T., & Moe, Y. A. (2010). Machine learning approach to automatic exudate detection in retinal images from diabetic patients. *Journal of Modern Optics,* 57(2), 124–135. https://doi.org/10.1080/09500340903118517

Southwell, B. J., Cheong, J. W., & Dempster, A. G. (2020). A Matched Filter for Spaceborne GNSS-R Based Sea-Target Detection. *IEEE Transactions on Geoscience and Remote Sensing* 58(8), 5922–5931. https://doi.org/10.1109/TGRS.2020.2973142

Spencer, T., Olson, J. A., McHardy, K. C., Sharp, P. F., & Forrester, J. v. (1996). An image-processing strategy for the segmentation and quantification of microaneurysms in fluorescein angiograms of the ocular fundus. *Computers and Biomedical Research,* 29(4), 284–302. https://doi.org/10.1006/cbmr.1996.0021

Staal, J., Abràmoff, M. D., Niemeijer, M., Viergever, M. A., & van Ginneken, B. (2004). Ridge-based vessel segmentation in color images of the retina. *IEEE Transactions on Medical Imaging* 23(4), 501–509. https://doi.org/10.1109/TMI.2004.825627

Suarez, M., Brea, V. M., Fernandez-Berni, J., Carmona-Galan, R., Cabello, D., & Rodriguez-Vazquez, A. (2017). Low-Power CMOS Vision Sensor for Gaussian Pyramid Extraction. *IEEE Journal of Solid-State Circuits,* 52(2), 483–495. https://doi.org/10.1109/JSSC.2016.2610580

Sudha, V., & Karthikeyan, C. (2018). Analysis of diabetic retinopathy using naive bayes classifier technique. *International Journal of Engineering & Technology*, 7(2.21), 440. https://doi.org/10.14419/ijet.v7i2.21.12462

Tang, M. C. S., Teoh, S. S., Ibrahim, H., &Embong, Z. (2021). Neovascularization detection and localization in fundus images using deep learning. *Sensors*, 21(16). https://doi.org/10.3390/s21165327

Tarr, J. M., Kaul, K., Chopra, M., Kohner, E. M., &Chibber, R. (2013). Pathophysiology of Diabetic Retinopathy. *ISRN Ophthalmology*, 2013, 1–13. https://doi.org/10.1155/2013/343560

Theeng Tamang, M. R., Sharif, M. S., Al-Bayatti, A. H., Alfakeeh, A. S., &Alsayed, A. O. (2020). A machine-learning-based approach to predict the health impacts of commuting in large cities: Case study of London. *Symmetry*, 12(5). https://doi.org/10.3390/SYM12050866

Theera-Umpon, N., Poonkasem, I., Auephanwiriyakul, S., &Patikulsila, D. (2020). Hard exudate detection in retinal fundus images using supervised learning. *Neural Computing and Applications*, 32(17), 13079–13096. https://doi.org/10.1007/s00521-019-04402-7

Tian, Y., Zhang, F., Qiu, Y., Wang, S., Li, F., Zhao, J., Pan, C., Tao, Y., Yu, D., & Wei, W. (2021). Reduction of choroidal neovascularization via cleavable VEGF antibodies conjugated to exosomes derived from regulatory T cells. *Nature Biomedical Engineering*, 5(9), 968–982. https://doi.org/10.1038/s41551-021-00764-3

Tolias, Y. A., &Panas, S. M. (1998). A fuzzy vessel tracking algorithm for retinal images based on fuzzy clustering. *IEEE Transactions on Medical Imaging*, 17(2), 263–273. https://doi.org/10.1109/42.700738

Tymchenko, B., Marchenko, P., &Spodarets, D. (2020). Deep learning approach to diabetic retinopathy detection. *ICPRAM 2020 - Proceedings of the 9th International Conference on Pattern Recognition Applications and Methods*, 501–509. https://doi.org/10.5220/0008970805010509

Valverde, C., Garcia, M., Hornero, R., & Lopez-Galvez, M. (2016). Automated detection of diabetic retinopathy in retinal images. *Indian Journal of Ophthalmology*, 64(1), 26–32. https://doi.org/10.4103/0301-4738.178140

van Netten, J. J., Bus, S. A., Apelqvist, J., Lipsky, B. A., Hinchliffe, R. J., Game, F., Rayman, G., Lazzarini, P. A., Forsythe, R. O., Peters, E. J. G., Senneville, É., Vas, P., Monteiro-Soares, M., & Schaper, N. C. (2020). Definitions and criteria for diabetic foot disease. *Diabetes/Metabolism Research and Reviews*, 36(S1). https://doi.org/10.1002/DMRR.3268

Verma, K., Deep, P., & Ramakrishnan, A. G. (2011). Detection and classification of diabetic retinopathy using retinal images. *Proceedings - 2011 Annual IEEE India Conference: Engineering Sustainable Solutions, INDCON-2011*, June. https://doi.org/10.1109/INDCON.2011.6139346

Vlachos, M., &Dermatas, E. (2010). Multi-scale retinal vessel segmentation using line tracking. *Computerized Medical Imaging and Graphics*, 34(3), 213–227. https://doi.org/10.1016/j.compmedimag.2009.09.006

Wang, D., Haytham, A., Pottenburgh, J., Saeedi, O., & Tao, Y. (2020). Hard Attention Net for Automatic Retinal Vessel Segmentation. *IEEE Journal of Biomedical and Health Informatics*, 24(12), 3384–3396. https://doi.org/10.1109/JBHI.2020.3002985

Wang, W., & Lo, A. C. Y. (2018). Diabetic retinopathy: Pathophysiology and treatments. *International Journal of Molecular Sciences*, 19(6). https://doi.org/10.3390/ijms19061816

Ward, L. (2019). Supervised Learning: Regression and Classification (Issue July). *US Department of Energy, Chicago*, 1–15.

Welikala, R. A. (2014). Automated Detection of Proliferative Diabetic Retinopathy from Retinal Images. *Journal of Medical Imaging and Health Informatics, September*.

Widyatmoko, A. C., Hardesty, B. D., & Wilcox, C. (2021). Detecting anchored fish aggregating devices (AFADs) and estimating use patterns from vessel tracking data in small-scale fisheries. *Scientific Reports*, 11(1). https://doi.org/10.1038/s41598-021-97227-1

Wisaeng, K., & Sa-Ngiamvibool, W. (2018). Automatic detection of exudates in retinal images using region-based, neighborhood and block operation. *Journal of Computer Science*, 14(4), 438–452. https://doi.org/10.3844/jcssp.2018.438.452

Xiao, L., Wu, B., & Hu, Y. (2020). Surface Defect Detection Using Image Pyramid. *IEEE Sensors Journal*, 20(13), 7181–7188. https://doi.org/10.1109/JSEN.2020.2977366

Yin, Y., Adel, M., &Bourennane, S. (2012). Retinal vessel segmentation using a probabilistic tracking method. *Pattern Recognition*, 45(4), 1235–1244. https://doi.org/10.1016/j.patcog.2011.09.019

Youssif, A. A. A., Ghalwash, A. Z., &Ghoneim, A. S. (2007). A Comparative Evaluation of Preprocessing Methods for Automatic Detection of Retinal Anatomy. *Proceedings of the Fifth International Conference on Informatics and Systems (INFOS9)*, May 2014, 24–30.

Zago, G. T. (2019). Diabetic Retinopathy Detection Based On Deep

Learning Universidade Federal do Espírito Santo) 1-12.

Zeng, X., Chen, H., Luo, Y., & Ye, W. (2019). Automated diabetic retinopathy detection based on binocular siamese-like convolutional neural network. *IEEE Access*, 7, 30744–30753. https://doi.org/10.1109/ACCESS.2019.2903171

Zhang, L., Li, Q., You, J., & Zhang, D. (2009). A modified matched filter with double-sided thresholding for screening proliferative diabetic retinopathy. *IEEE Transactions on Information Technology in Biomedicine*, 13(4), 528–534. https://doi.org/10.1109/TITB.2008.2007201

Zhou, C., Zhang, X., & Chen, H. (2020). A new robust method for blood vessel segmentation in retinal fundus images based on weighted line detector and hidden Markov model. *Computer Methods and Programs in Biomedicine*, 187. https://doi.org/10.1016/j.cmpb.2019.105231

APPENDIX

SOURCE CODE

```matlab
clc;
clear;

for n=1:516
im{n}        = imread(sprintf('IDRiD_0%d.jpg',n));
img           = im{n};

gray_scale     = rgb2gray(img);
   J             = imadjust(gray_scale);
Kmedian       = medfilt2(J);
   I              = imresize(Kmedian,[750 498]);

% Scale Images using pyramid
% Define the number of pyramid levels
levels = 3;

% Create an empty cell array to store the pyramid levels
```

```matlab
pyramid = cell(1, levels+1);
pyramid{1} = img;

% Loop over the number of levels
for i = 2:levels+1
 % Apply a Gaussian filter to the previous level
img = imfilter(pyramid{i-1}, fspecial('gaussian', [5 5], 1));
% Downsample the filtered image
img = imresize(img, 0.5);
% Append the filtered and downsampled image to the pyramid cell array pyramid{i}
= img;
end

% Display the pyramid levels
for i = 1:levels+1
figure, imshow(pyramid{i});
end

%Extracting LBP for first scaled images
    features      = extractLBPFeatures(I);
numNeighbuors  = 8;
numBins        = numNeighbours*(numNeighbours-1)+3;
lbpCellHists  = reshape(features, numBins,[]);
lbpCellHists  = bsxfun(@rdivide,lbpCellHists,sum(lbpCellHists));
    features      = reshape(lbpCellHists,1,[]);

%LBP for second scaled images
features1     = extractLBPFeatures(I1,'Normalization','None');
  numNeighbours1 = 8;
  numBins1      = numNeighbours1*(numNeighbours1-1)+3;
  lbpCellHists1 = reshape(features1,numBins1,[]);
```

```matlab
    lbpCellHists1 = bsxfun(@rdivide,lbpCellHists1,sum(lbpCellHists1));
    features1     = reshape(lbpCellHists1,1,[]);


%LBP for third scaled images
features2     = extractLBPFeatures(I2,'Normalization','None');
    numNeighbours2 = 8;
    numBins2      = numNeighbours2*(numNeighbours2-1)+3;
    lbpCellHists2 = reshape(features2,numBins2,[]);
    lbpCellHists2 = bsxfun(@rdivide,lbpCellHists2,sum(lbpCellHists2));
    features2     = reshape(lbpCellHists2,1,[]);



%Merge all scaled image features
CombinedLBP   = [features features1 features2];
    merge(n,:)    = CombinedLBP;


end
merge;
base_path = 'C:\Users\Yunusa\Desktop\Yunusa project';


% Save extracted features in CSV
myFiles = fullfile(base_path,sprintf('DRfeature%d.csv',n));
csvwrite(myFiles,merge)



%80:20
%Load dataset
X = DRfeature516(1:516,:);
Y = labels(1:516,:);


%80:20 slipt
```

```matlab
rand_num    = randperm(516);


x_train    = X(rand_num(1:413),:);
y_train    = Y(rand_num(1:413),:);


x_test    = X(rand_num(414:end),:);
y_test    = Y(rand_num(414:end),:);
```

%% Classifier Model
```matlab
mdltree    = fitctree(x_train,y_train);
mdlecoc    = fitcecoc(x_train,y_train);
```

%Accuracy
```matlab
acctree    = sum(predict(mdltree,x_test)== y_test)/length(y_test)*100;
accecoc    = sum(predict(mdlecoc,x_test)== y_test)/length(y_test)*100;
```

%Confusion Matrix
```matlab
tree_te = predict(mdltree,x_test); tree_Con  = confusionmat(y_test,tree_te);
ecoc_te = predict(mdlecoc,x_test); ecoc_Con  = confusionmat(y_test,ecoc_te);
```

%Rows and Columns of the confusion matrix of Decision Tree
```matlab
tree_con1=tree_Con(1:1,1:1);     tree_con2 = tree_Con(1:1,2:2);
tree_con3 = tree_Con(1:1,3:3);  tree_con16 = tree_Con(1:1,4:4);
tree_con17 = tree_Con(1:1,5:5); tree_con4 = tree_Con(2:2,1:1);
tree_con5 = tree_Con(2:2,2:2);  tree_con6 = tree_Con(2:2,3:3);
tree_con18 = tree_Con(2:2,4:4); tree_con19 = tree_Con(2:2,5:5);
tree_con7 = tree_Con(3:3,1:1);  tree_con8 = tree_Con(3:3,2:2);
tree_con9 = tree_Con(3:3,3:3);  tree_con20 = tree_Con(3:3,4:4);
tree_con21 = tree_Con(3:3,5:5);  tree_con10= tree_Con(4:4,1:1);
tree_con11= tree_Con(4:4,2:2);  tree_con12= tree_Con(4:4,3:3);
tree_con22 = tree_Con(4:4,4:4); tree_con23 = tree_Con(4:4,5:5);
```

```
tree_con13=  tree_Con(5:5,1:1);  tree_con14=  tree_Con(5:5,2:2);
tree_con15= tree_Con(5:5,3:3);  tree_con24 = tree_Con(5:5,4:4);
tree_con25 = tree_Con(5:5,5:5);
```

%Rows and Columns of the confusion matrix of ECOC
```
ecoc_con1 = ecoc_Con(1:1,1:1);   ecoc_con2 = ecoc_Con(1:1,2:2);
ecoc_con3 = ecoc_Con(1:1,3:3);   ecoc_con16 = ecoc_Con(1:1,4:4);
ecoc_con17 = ecoc_Con(1:1,5:5);  ecoc_con4 = ecoc_Con(2:2,1:1);
ecoc_con5 = ecoc_Con(2:2,2:2);   ecoc_con6 = ecoc_Con(2:2,3:3);
ecoc_con18 = ecoc_Con(2:2,4:4);  ecoc_con19 = ecoc_Con(2:2,5:5);
ecoc_con7 = ecoc_Con(3:3,1:1);   ecoc_con8 = ecoc_Con(3:3,2:2);
ecoc_con9 = ecoc_Con(3:3,3:3);   ecoc_con20 = ecoc_Con(3:3,4:4);
ecoc_con21 = ecoc_Con(3:3,5:5);  ecoc_con10= ecoc_Con(4:4,1:1);
ecoc_con11= ecoc_Con(4:4,2:2);   ecoc_con12= ecoc_Con(4:4,3:3);
ecoc_con22 = ecoc_Con(4:4,4:4);  ecoc_con23 = ecoc_Con(4:4,5:5);
ecoc_con13= ecoc_Con(5:5,1:1);   ecoc_con14= ecoc_Con(5:5,2:2);
ecoc_con15= ecoc_Con(5:5,3:3);   ecoc_con24 = ecoc_Con(5:5,4:4);
ecoc_con25 = ecoc_Con(5:5,5:5);
```

%TP, TN, FP, FN
```
tree_TP = tree_con1; tree_FP = tree_con2+tree_con3+ tree_con16+ tree_con17;
tree_FN=tree_con4+tree_con7 +tree_con10 + tree_con13;
tree_TN = tree_con5+ tree_con6+
tree_con18+tree_con19+tree_con8+tree_con9+tree_con20+tree_con21+tree_con1
0+tree_con12+...
   tree_con22+tree_con23+tree_con14+tree_con15+tree_con24+tree_con25;

ecoc_TP = ecoc_con1; ecoc_FP = ecoc_con2+ecoc_con3+ ecoc_con16+
ecoc_con17; ecoc_FN=ecoc_con4+ecoc_con7 +ecoc_con10 + ecoc_con13;
ecoc_TN = ecoc_con5+ ecoc_con6+
ecoc_con18+ecoc_con19+ecoc_con8+ecoc_con9+ecoc_con20+ecoc_con21+ecoc
```

```
_con10+ecoc_con12+...
    ecoc_con22+ecoc_con23+ecoc_con14+ecoc_con15+ecoc_con24+ecoc_con25;



%Precision and recall for class 1
tree_precision = tree_con1/(tree_con1+ tree_con2);
tree_recall    = tree_con1/(tree_con1+tree_con4);
ecoc_precision = ecoc_con1/(ecoc_con1+ecoc_con2);
ecoc_recall    = ecoc_con1/(ecoc_con1+ecoc_con4);


%Precision and recall for class 2
tree_precision_B = tree_con5/(tree_con5+ tree_con6);
tree_recall_B    = tree_con5/(tree_con5+tree_con8);
ecoc_precision_B = ecoc_con5/(ecoc_con5+ecoc_con6);
ecoc_recall_B    = ecoc_con5/(ecoc_con5+ecoc_con8);


%Precision and recall for class 3
tree_precision_C = tree_con9/(tree_con7+ tree_con9);
tree_recall_C    = tree_con9/(tree_con3+tree_con9);
ecoc_precision_C = ecoc_con9/(ecoc_con7+ecoc_con9);
ecoc_recall_C    = ecoc_con9/(ecoc_con3+ecoc_con9);


%Precision and recall for class 4
tree_precision_D = tree_con22/(tree_con10+ tree_con22);
tree_recall_D    = tree_con22/(tree_con16+tree_con22);
ecoc_precision_D = ecoc_con22/(ecoc_con10+ecoc_con22);
ecoc_recall_D    = ecoc_con22/(ecoc_con16+ecoc_con22+);


%Precision and recall for class 5
tree_precision_E = tree_con25/(tree_con13+ tree_con25);
tree_recall_E    = tree_con25/(tree_con17+tree_con25);
```

ecoc_precision_E = ecoc_con25/(ecoc_con13+ecoc_con25);
ecoc_recall_E   = ecoc_con25/(ecoc_con17+ecoc_con25);

%Averaging Precision and recall
tree_precision_aver = (tree_precision_A + tree_precision_B + tree_precision_C +
tree_precision_D + tree_precision_E) / 5
tree_recall_aver   = (tree_recall_A + tree_recall_B + tree_recall_C + tree_recall_D +
tree_recall_E) /5

ecoc_precision_aver = (ecoc_precision_A + ecoc_precision_B + ecoc_precision_C +
ecoc_precision_D + ecoc_precision_E) / 5

ecoc_recall_aver   = (ecoc_recall_A + ecoc_recall_B + ecoc_recall_C +
ecoc_recall_D + ecoc_recall_E) / 5

%F-Score for class 1
tree_fscore = 2*((tree_precision*tree_recall)/(tree_precision+tree_recall));
ecoc_fscore = 2*((ecoc_precision*ecoc_recall)/(ecoc_precision+ecoc_recall));

%F-Score for class 2
tree_fscore_B =
2*((tree_precision_B*tree_recall_B)/(tree_precision_B+tree_recall_B));
ecoc_fscore_B =
2*((ecoc_precision_B*ecoc_recall_B)/(ecoc_precision_B+ecoc_recall_B));

%F-Score for class 3
tree_fscore_C =
2*((tree_precision_C*tree_recall_C)/(tree_precision_C+tree_recall_C));
ecoc_fscore_C =
2*((ecoc_precision_C*ecoc_recall_C)/(ecoc_precision_C+ecoc_recall_C));

%F-Score for class 4

tree_fscore_D =
2*((tree_precision_D*tree_recall_D)/(tree_precision_D+tree_recall_D));
ecoc_fscore_D =
2*((ecoc_precision_D*ecoc_recall_D)/(ecoc_precision_D+ecoc_recall_D));

%F-Score for class 5

tree_fscore_E =
2*((tree_precision_E*tree_recall_E)/(tree_precision_E+tree_recall_E));
ecoc_fscore_E =
2*((ecoc_precision_E*ecoc_recall_E)/(ecoc_precision_E+ecoc_recall_E));

%Averaging F-score

tree_fscore_aver   = (tree_ fscore _A + tree_ fscore _B + tree_ fscore _C + tree_ fscore _D + tree_ fscore _E) /5
ecoc_ fscore _aver = (ecoc_ fscore _A + ecoc_ fscore _B + ecoc_ fscore _C + ecoc_ fscore _D + ecoc_ fscore _E) / 5